LEVEL

NOSC

NOSC TR 387

NOSC TR 387

Technical Report 387

NAVAL BLUE-GREEN SINGLE-PULSE DOWNLINK PROPAGATION MODEL

Technical Advisor to the Blue-Green
Optical Communication Program
Joint Coordinating Committee

1 January 1979

Final Report: January 1978 — December 1978

Prepared for
Naval Electronic Systems Command

APPROVED FOR PUBLIC RELEASE; DISTRIBUTION UNLIMITED.

NAVAL OCEAN SYSTEMS CENTER
SAN DIEGO, CALIFORNIA 92152

NAVAL OCEAN SYSTEMS CENTER, SAN DIEGO, CA 92152

AN ACTIVITY OF THE NAVAL MATERIAL COMMAND

RR GAVAZZI, CAPT, USN
Commander

HL BLOOD
Technical Director

ADMINISTRATIVE INFORMATION

The analytical model for blue-green pulse propagation reported within this document was the result of the combined efforts of Dr. P. J. Titterton and H. E. Sweeney of GTE Sylvania, R. D. Anderson, R. F. Howarth, M. E. Hyde and L. B. Stotts of the Naval Ocean Systems Center, and W. R. Stone of the MEGATEK Corporation. The authors would like to thank Mr. M. L. Parker, Jr., Naval Electronics System Command, Code 3102, for his initiation, interest and support of this work.

Released by
LCDR S. E. Dollar, Head
Communications Research
and Technology Division

Under Authority of
R. H. DuBois, Head
Communication Systems
and Technology Department

UNCLASSIFIED

SECURITY CLASSIFICATION OF THIS PAGE (When Data Entered)

REPORT DOCUMENTATION PAGE

READ INSTRUCTIONS BEFORE COMPLETING FORM

1. REPORT NUMBER: NOSC Technical Report 387 (TR 387)

2. GOVT ACCESSION NO.

3. RECIPIENT'S CATALOG NUMBER

4. TITLE (and Subtitle): NAVAL BLUE-GREEN SINGLE-PULSE DOWNLINK PROPAGATION MODEL

5. TYPE OF REPORT & PERIOD COVERED: Final Report, Jan [illegible]-Dec [illegible]78

6. PERFORMING ORG. REPORT NUMBER

7. AUTHOR(s): Technical Advisor to the Blue-Green Optical Communication Program Joint Coordinating Committee

8. CONTRACT OR GRANT NUMBER(s): 89p.

9. PERFORMING ORGANIZATION NAME AND ADDRESS: Naval Ocean Systems Center, San Diego, CA 92152

10. PROGRAM ELEMENT, PROJECT, TASK AREA & WORK UNIT NUMBERS: CM06

11. CONTROLLING OFFICE NAME AND ADDRESS: Naval Electronic Systems Command, Washington, DC 20360

12. REPORT DATE: 1 Jan [illegible]79

13. NUMBER OF PAGES: 87

14. MONITORING AGENCY NAME & ADDRESS (if different from Controlling Office)

15. SECURITY CLASS. (of this report): Unclassified

15a. DECLASSIFICATION/DOWNGRADING SCHEDULE

16. DISTRIBUTION STATEMENT (of this Report)

Approved for public release; distribution unlimited

14 NOSC/TR-387

17. DISTRIBUTION STATEMENT (of the abstract entered in Block 20, if different from Report)

18. SUPPLEMENTARY NOTES: 10 P. J./Titterton, V. E./Sweeney, R. D. Anderson, R. F./Howarth, M. E./Hyde

19. KEY WORDS (Continue on reverse side if necessary and identify by block number)

20. ABSTRACT (Continue on reverse side if necessary and identify by block number)

This technical report describes the official Navy model for signal and noise characteristics of a single blue-green optical pulse propagated from a satellite laser source to a submerged receiver in all weather conditions.

A mathematical model is developed in two groups: the signal group relates the instantaneous received optical signal power, while, the noise group relates the total noise equivalent optical power to the noise source. Both groups of the model account for propagation path and receiver characteristics; and, they allow calculation of the signal-to-noise ratio for any blue-green single-pulse downlink from a satellite laser source to a submerged receiver. The relative technical uncertainty in accuracy of both equation groups has also been included.

DD FORM 1 JAN 73 1473 EDITION OF 1 NOV 65 IS OBSOLETE S/N 0102-LF-014-6601

UNCLASSIFIED

SECURITY CLASSIFICATION OF THIS PAGE (When Data Entered)

393 159

SUMMARY

OBJECTIVE

Develop a mathematical model for the noise and signal characteristics involved in the propagation of a single blue-green optical pulse from a satellite laser source to a submerged receiver under all weather conditions.

RESULTS

A mathematical model is developed in two groups: the signal group relates the instantaneous received optical signal power, while, the noise group relates the total noise equivalent optical power to the noise source. Both groups of the model account for propagation path and receiver characteristics; and, they allow calculation of the signal-to-noise ratio for any blue-green downlink from a satellite laser source to a submerged receiver. The relative technical uncertainty in accuracy of both equation groups has also been included.

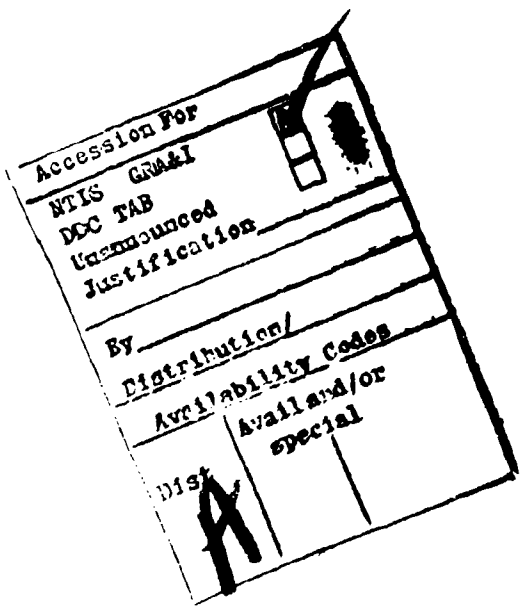

CONTENTS

CONTENTS (Continued)

ILLUSTRATIONS

CONTENTS (Continued)

TABLES

CONTENTS (Continued)

1.0 INTRODUCTION

The Navy has long recognized that the so-called "blue-green window" for optical propagation through sea water offers a potential communication channel for information transfer to submarines at operational depth and speed. This recognition has spurred continuing efforts to develop a technology base in blue-green propagation and devices. This report is the initial documentation of the official Navy model for the signal and noise characteristics of a single blue-green optical pulse, propagating from a satellite laser source to a submarine receiver in all weather conditions.

The model is divided into two groups of equations: the signal group relates the instantaneous received optical signal power, while, the noise group relates the total noise equivalent optical power to the source. Both groups of the model account for propagation path and receiver characteristics; and, they allow calculation of the SNR for any single-pulse blue-green downlink from a satellite laser source to a submerged receiver.

Figure 1 shows all the input parameters for each portion of the signal group. The laser pulse originates at the satellite, propagates through the atmosphere (including whatever clouds are present), the air-sea interface, the ocean water, and is finally detected by the submerged receiver. With noise, some of the background light sources (sun and moon) follow a like path, while others (blue skylight and star/zodiacal light) are not point-like beam sources and must be treated differently. Finally, the bioluminescent light originates in the water itself and is not effected by atmospheric properties.

In this report, sections 2.0 and 3.0 relate the model and are organized in the following manner. First, the method of approach used in each group is briefly discussed and a detailed flow chart (figs 3, 20 respectively) showing the interrelations between all the equations is illustrated. The second subsections (2.2 and 3.2) define and discuss all input information needed to perform the calculations. The third and final subsections (2.3 and 3.3) contain the derivations and justifications of all equations used. These equations and derivations are discretely organized in a modular fashion, so future revisions (e.g., cloud and water) may be made without major dislocations to the model.

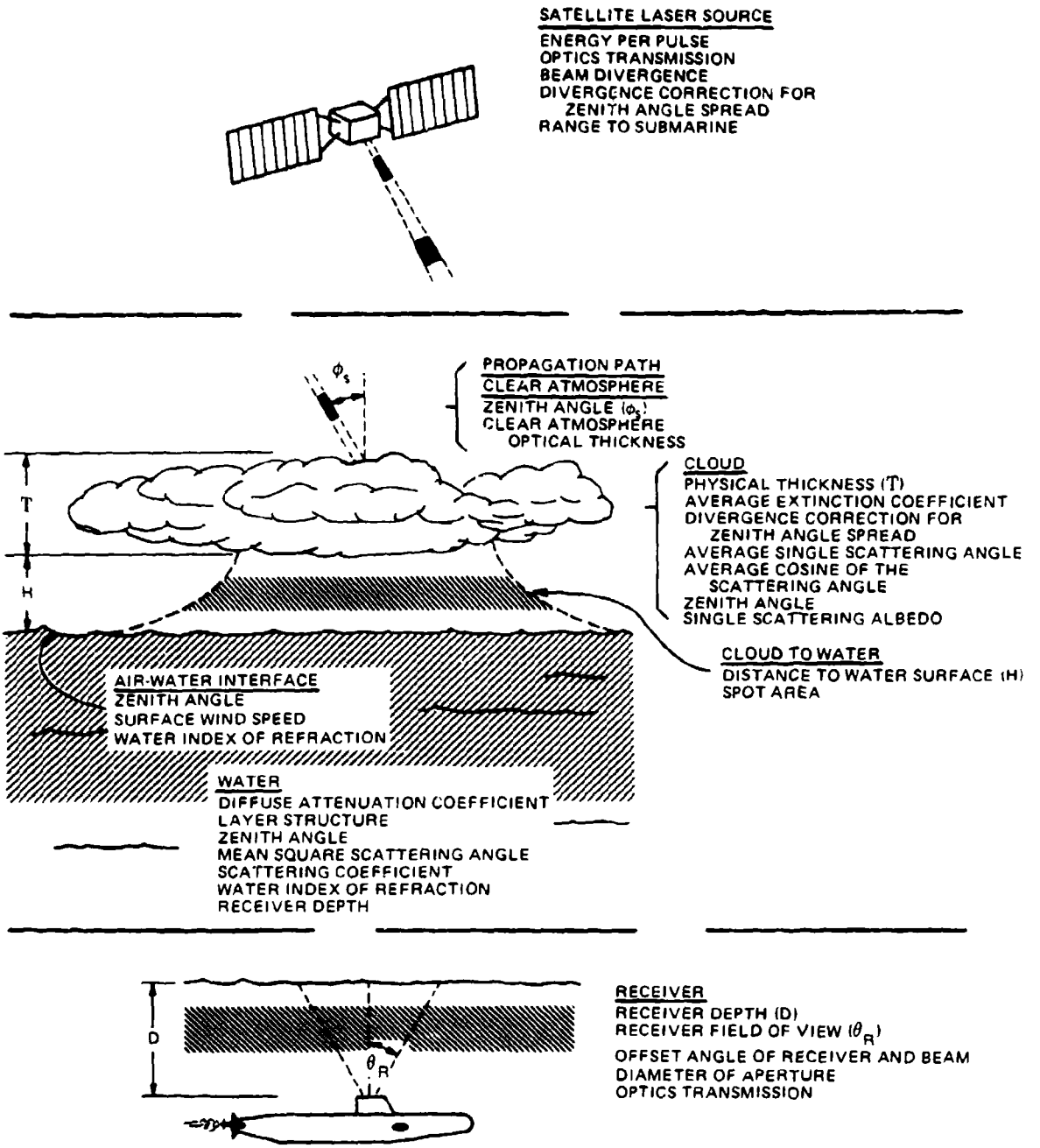

Figure 1. Parameters for the single-pulse downlink model.

2.0 SIGNAL PROPAGATION GROUP

This section discusses the equation group for the optical propagation of a single blue-green signal pulse from a satellite to a submerged receiver. The output of the signal group is combined with that of the noise group, to define the signal to noise ratio (SNR) for a given communication.

2.1 OBJECTIVE, STRUCTURE AND FUNCTION

This section describes the basic approach used with the detailed single pulse downlink signal propagation group and presents a flow chart showing the interrelationships of the sub-models and their required inputs.

2.1.1 Philosophy of Approach

The signal group is organized in a modular fashion, so that the effect of each portion of the path is evident. In addition, as further experiments and analyses are undertaken, pieces of the model may be upgraded without requiring extensive modification of the total model. The signal calculation group considers the following three properties of the signal and separately models the effects of the propagation path on each:

(a) the energy transmission from the satellite transmitter to the submerged receiver,

(b) the distribution of the signal radiance at the submarine receiver, and

(c) the pulse shape and width at the submarine receiver.

These three properties are then combined to yield the instantaneous received optical power at the surface of the submerged photodetector.

This approach does not attempt to treat all possible cloud conditions. Rather, a break point is established at a minimum optical thickness of 10. Below that value, one set of sub-models is assumed to apply, while above it a different set applies. In many cases, these sub-models do not correspond at τ_{opt} = optical thickness = 10, and so the overall model should only be used for $\tau_{opt} < 10$ and $\tau_{opt} > 10$. (Future analysis and experiments on the "multiple-forward scattering" region should enable the sub-models to be upgraded, removing this inconsistency.

Finally, simple analytic forms are assumed for at-present unknown functions such as the radiance distribution, and pulse shape and width. This enables production of analytic results (except for the receiver axis off-set from the beam axis of the incident radiance), which are an aid to a physical understanding of the overall propagation problem.

2.1.2 Signal Group Structure

A schematic of the overall signal propagation group is presented in figure 2. Given the input parameters, the pulse width, shape, and angular and radiance distribution are derived. Then, using the angular and radiance distribution, and the input data, the energy transmission of the path is calculated. Finally, given the energy transmission and the received pulse shape, the signal (instantaneous received power) is calculated.

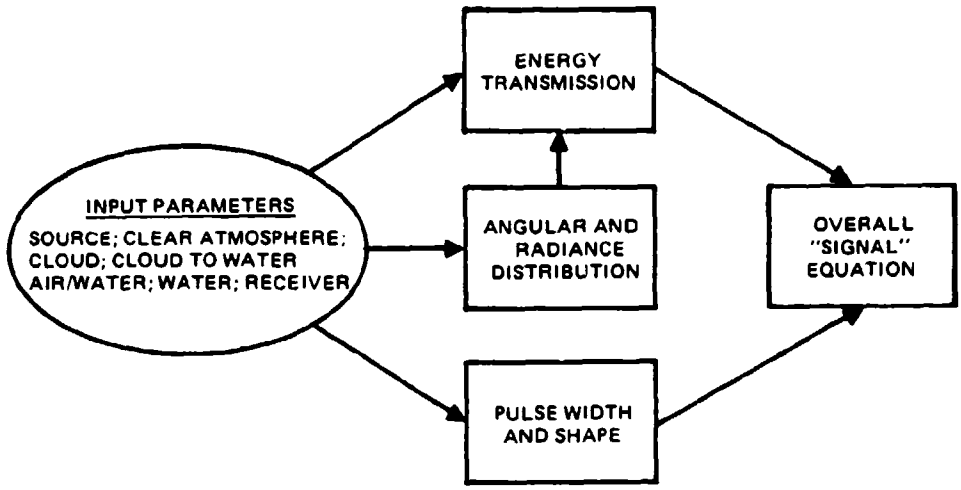

Figure 2. Schematic of single-pulse downlink signal propagation group.

Figure 3 is a detailed flow diagram showing the calculations that must be performed to arrive at the required output. The following five steps are used to exercise the signal propagation group:

- The input parameters are listed in the seven ellipses on the left hand side of the figure, including source, clear atmosphere, cloud, cloud to water, air-water interface, water, and receiver parameters. (The symbols are defined in the glossary and also in the input discussion in section 2.2).
- The primary calculation equations are represented by the rectangular boxes. Within each box is the symbol for the parameter to be calculated and the equation number (from section 2.3) for the equation to be used to calculate the parameter. The first quantity calculated is the cloud optical thickness, τ_{opt}, since this determines the equations to be used to calculate many other parameters. Whenever // appears in a rectangular box, the equation number preceding it refers to $\tau_{opt} > 10$, while the equation number following it refers to $\tau_{opt} < 10$. Hence, given the value of τ_{opt} the rest of the models to be used are specifically determined.
- The second set of calculations performed are of three types:

  (a) path transmission, including τ_a, τ_c, τ_{cw}, τ_{aw} and τ_w;

  (b) pulse width and shape, including Δt_c, Δt_{cw}, Δt_w and t_M;

  (c) angular and radiance distribution, including f_A, f_{AW}, f_W, ϕ_o and $f(\theta_R \phi_o, \delta)$.
- The path transmission, angular and radiance distribution, source and receiver parameters are then used to calculate the received energy, E_R.
- The received energy, pulse width and shape are used to calculate the instantaneous received power $P_R(t)$.

The computer program to be developed will follow the flow chart in figure 3.

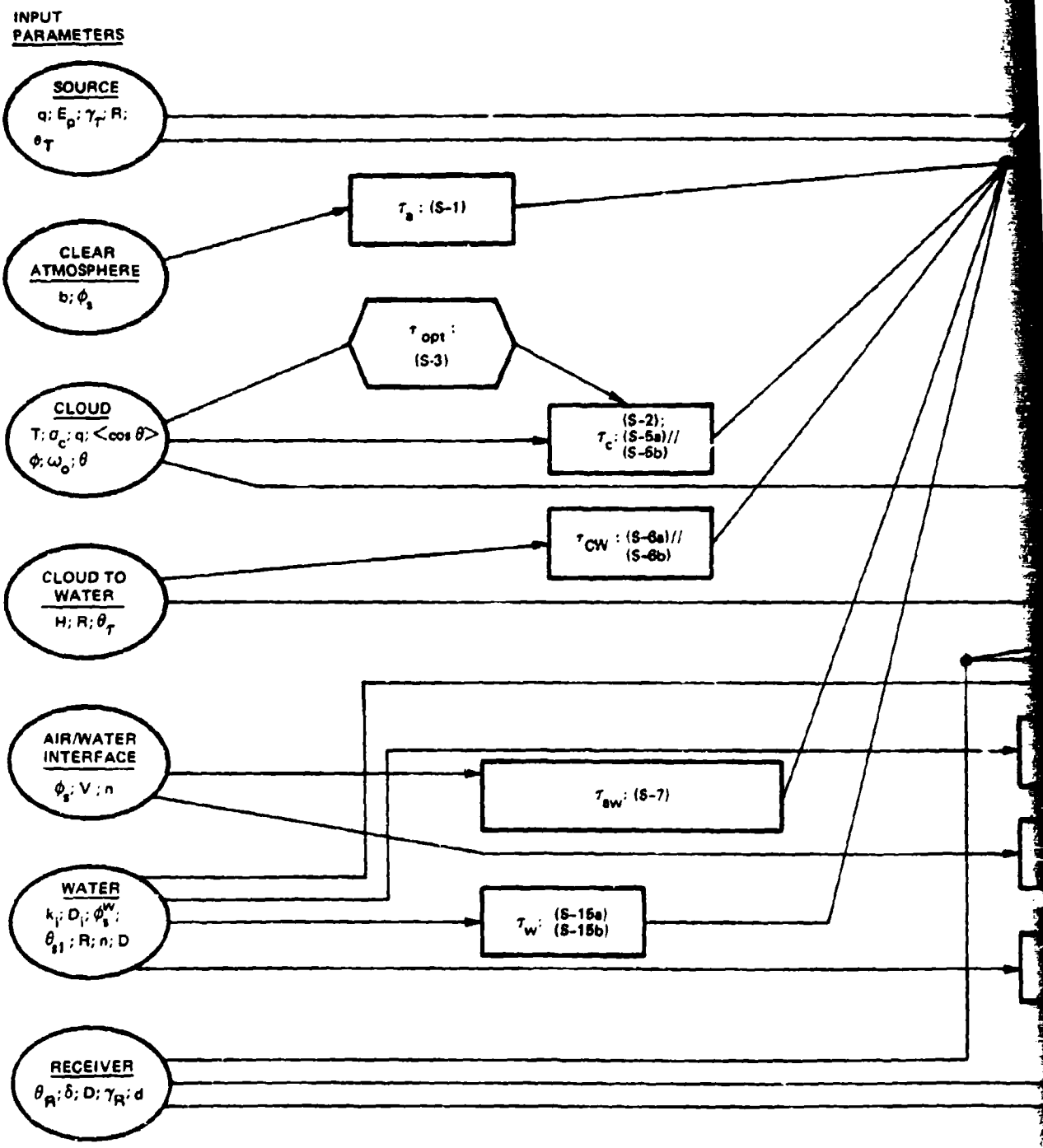
INPUT PARAMETERS
SOURCE
q; E_p; γ_T; R; θ_T
CLEAR ATMOSPHERE
b; ϕ_s
τ_a : (S-1)
τ_{opt} : (S-3)
CLOUD
T; σ_c; q; <cos θ>
ϕ; ω_o; θ
(S-2); τ_c: (S-5a)// (S-5b)
τ_{CW} : (S-6a)// (S-6b)
CLOUD TO WATER
H; R; θ_T
AIR/WATER INTERFACE
ϕ_s; V ; n
τ_{aw}: (S-7)
WATER
k_i; D_i; ϕ_s^w; θ_{s1} ; R; n; D
τ_w: (S-15a) (S-15b)
RECEIVER
θ_R; δ; D; γ_R; d

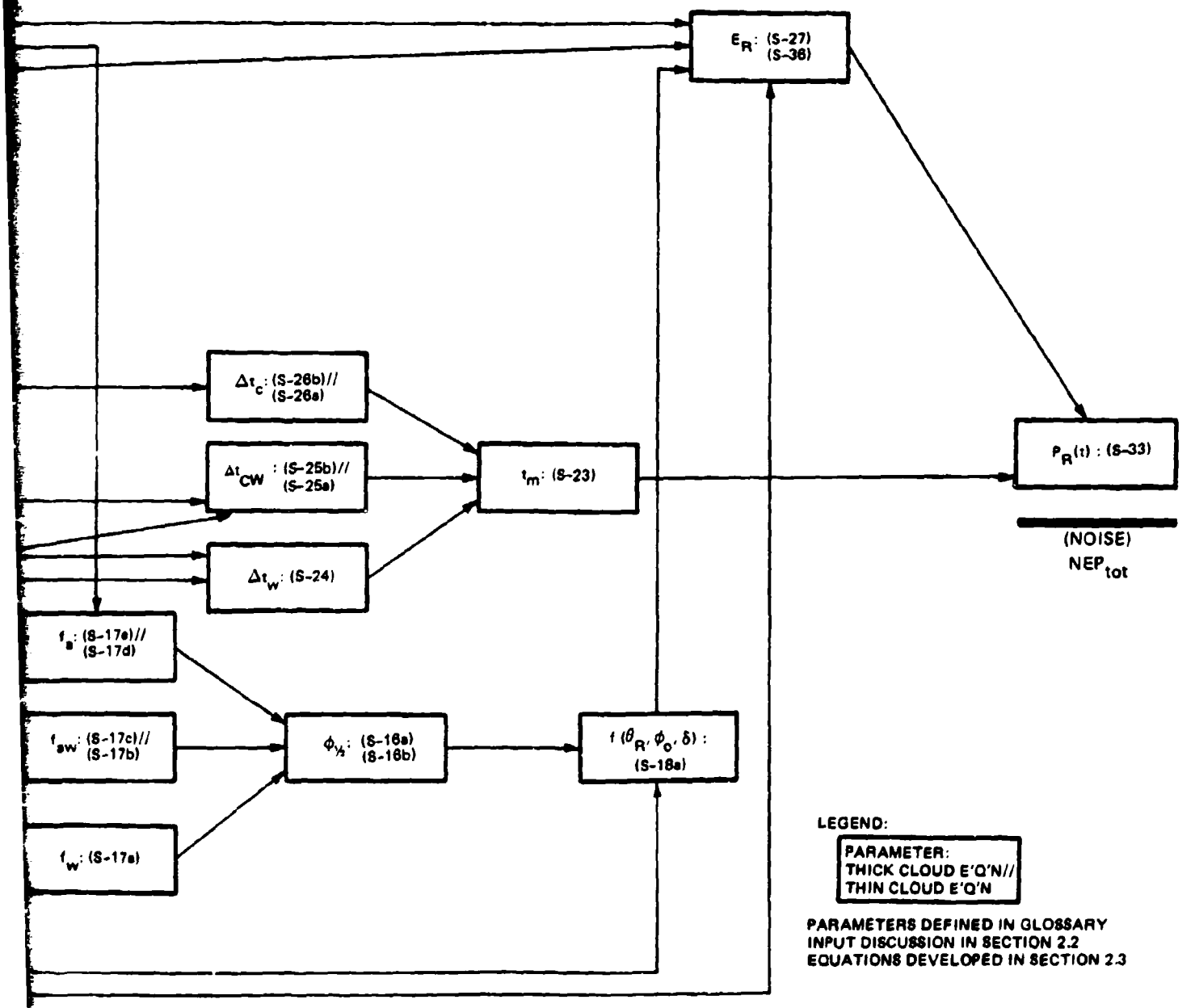

Figure 3. Flow diagram of single-pulse downlink signal propagation group.

2.2 INPUT FOR SIGNAL CALCULATION

This section discusses the form of the required inputs to the single pulse downlink signal propagation model, in terms of the seven categories: source, clear atmosphere, cloud, cloud to water, air-water interface, water and receiver.

2.2.1 Source

The required source parameters are:

Symbol	Description	Units
q	A parameter describing the ability of the satellite transmitter to correct for the geometric zenith angle spreading of the spot. q = 0 implies the spot remains the same area, independent of zenith angle, while q = 1 means the spot grows naturally with zenith angle. Hence, $0 \leq q \leq 1$.	
E_p	Energy per pulse of the transmitter laser.	Joules
γ_T	Transmission of the transmitter optical chain.	
R	Range from the satellite transmitter to the submarine receiver.	metres
θ_T	Full angle beam divergence to the e^{-2} irradiance points of the transmitter beam.	radians

2.2.2 Clear Atmosphere

The required parameters are:

Symbol	Description	Units
b	Effective clear atmosphere optical thickness such that for a 70 percent-zenith transmission, b = 0.357	
ϕ_s	In-air transmitter zenith angle	radians

2.2.3 Cloud

The required parameters are:

Symbol	Description	Units
T	Geometric or physical thickness of the cloud	metres
σ_c	Average extinction coefficient of the cloud	$(\text{metres})^{-1}$
q	A parameter describing the ability of the satellite transmitter to correct for the geometric zenith angle spreading of the spot. q = 0 implies the spot remains the same area independent of zenith angle, while q = 1 means the spot grows naturally with zenith angle. Hence $o \leq q \leq 1$.	
$\langle \cos \theta \rangle$	The average value of the cosine of the scattering angle for single scattering within the cloud	
ϕ_s	In-air transmitter zenith angle	radians

Symbol	Description	Units
ω_o	The single scattering albedo of the cloud particles, or, the ratio of the probability of scattering to the probability of extinction for a single scattering event.	
θ	The average angle for single scattering within the cloud	radians

2.2.4 Cloud to Water

The required parameters are:

Symbol	Description	Units
H	Distance from cloud base to water to surface	metres
R	Range from the satellite transmitter to the submarine receiver	metres
θ_T	Full angle beam divergence to the e^{-2} irradiance points of transmitted beam	radians

2.2.5 Air-Water Interface

The required parameters are:

Symbol	Description	Units
ϕ_s	In-air transmitter zenith angle	radians
v	Surface wind speed	metres/ second
n	Water index of refraction	

2.2.6 Water

The required parameters are:

Symbol	Description	Units
k_i	Diffuse attenuation coefficient of the i'th water layer	$(\text{metres})^{-1}$
D_i	Thickness of the i'th water layer	metres
ϕ_s^w	In-water transmitter zenith angle	radians
θ_{si}	Root-mean-square angle for a single scattering event in the water	radians
s	Scattering coefficient for the entire water path	$(\text{metres})^{-1}$
n	Water index of refraction	
D	Depth of the submarine receiver	metres

2.2.7 Receiver

The required parameters are:

Symbol	Description	Units
θ_R	Half-angle of the receiver field of view	radians
δ	Off-set angle between the in-water signal beam axis and the receiver optical axis	radians
D	Depth of the submarine receiver	metres
γ_R	Transmission of the receiver optical chain	
d	Diameter of the receiver optical aperture	metres

2.3 SIGNAL CALCULATION MODULES

This section develops all the equations used in the calculation of the instantaneous received signal power. Sections 2.3.1, 2.3.2, 2.3.3, 2.3.4, 2.3.6 and 2.3.7 consider the path transmission of the energy. Sections 2.3.5 and 2.3.8 consider the angular effects and the distribution of the received radiance. Section 2.3.9 considers the received pulse shape and width. In each of these sections, after the equations are developed they are evaluated for typical cases in both tables and figures. Section 2.3.10 combines the previous results to obtain the received energy and the optical signal power.

2.3.1 Clear Atmospheric Transmission

In the absence of any clouds or aersols, the clear atmospheric transmission is described by the term τ_a. Using the approximate AFCRL model (ref 1), the signal zenith angle dependence is given by:

$$\boxed{\tau_a = \exp\left[-b\sec\phi_s\right]} \quad , \tag{S-1}$$

for

τ_a = signal clear atmospheric transmission,

b = effective clear atmospheric optical thickness, and

ϕ_s = signal zenith angle.

The typical value of b is determined from:

$$\tau_a(\phi_s = 0) = 0.7 = \exp(-b) \quad ,$$

or

$$b = 0.357 \quad .$$

Table 1 and figure 4 show the values of τ_a as a function of signal zenith angle.

---

1. AFCRL-71-0279, Optical Properties of the Atmosphere (Revised), by RA McClatchey, RW Fenn, JEA Selby, FE Volz, and JS Garing, 10 May 1971.

Table 1. Typical clear atmospheric transmission (b = 0.357).

ϕ_s, Single Zenith Angle (degrees)	τ_a, Clear Atmospheric Transmission
0	0.7
10	0.7
20	0.68
30	0.66
40	0.63
50	0.57
60	0.49
70	0.35
80	0.13

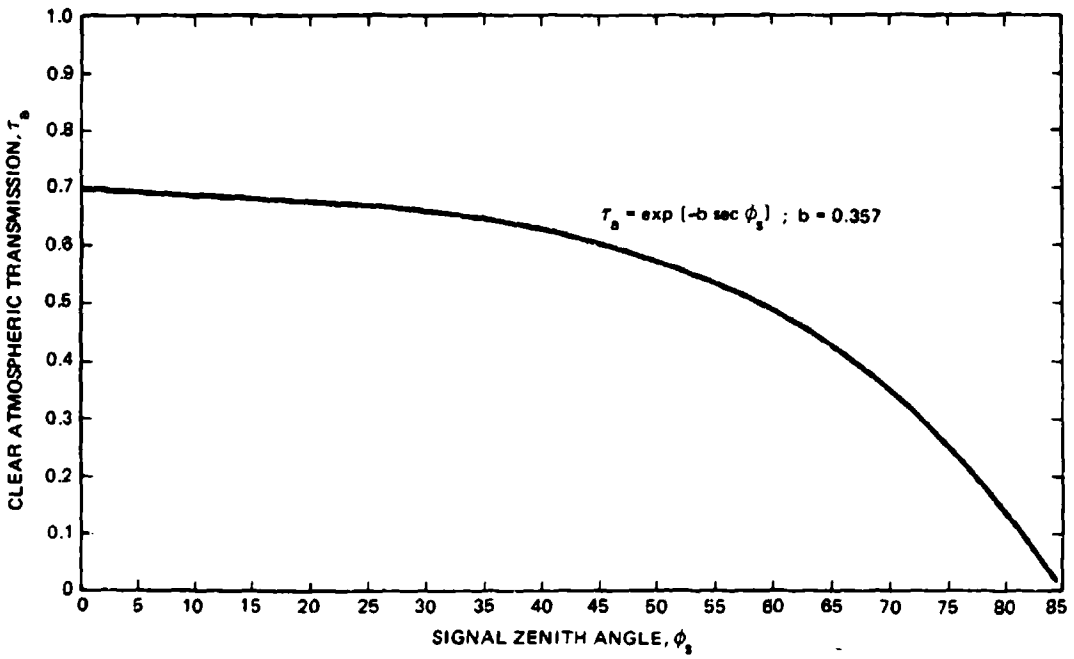

Figure 4. Typical clear atmospheric transmission (b = 0.357).

2.3.2 Cloud Energy Transmission

Insofar as they affect optical propagation, clouds may be categorized as negligible to very thin, thin, and thick. There are no verified experimental results that treat any one of these three classes. Since we are discussing an energy transmission here, and most analyses and partial experiments are in terms of the transmitted irradiance (energy/second/area), there are few analytic expressions for the cloud energy transmission.

Our decision is to treat only two classes: thick clouds and nearly clear weather. We do this with the understanding that evaluating the model near the transition point will yield results that are incorrect in principle, and so only for small and large optical thickness (defined below) should the overall model be expected to apply.

We propose to adopt the multiple-scattering Monte-Carlo derived diffusion-like expression of Bucher (ref 2) and Van der Hulst (ref 3) for thick clouds, so that at zenith:

$$\tau_c = \frac{1.69}{\tau_{opt}\,(1 - \langle\cos\theta\rangle) + 1.42} \quad , \tag{S-2}$$

where

τ_c = signal energy transmission through the cloud,

τ_{opt} = optical thickness of the cloud, and

$\langle\cos\theta\rangle$ = mean cosine of the scattering angle.

In discussing this equation, Bucher has estimated that the numerical parameters (1.69 and 1.42) are uncertain to within factors of 2X.

The optical thickness of the cloud, for a homogeneous cloud, is given by:

$$\tau_{opt} = T\,\sigma_c \quad , \tag{S-3}$$

where

T = geometrical thickness of the cloud, and

σ_c = mean extinction coefficient of the cloud.

As a typical example, for a strato-cumulus cloud, we might have T = 1200 m and $\sigma_c = 0.04\ m^{-1}$, so $\tau_{opt} = 48$. For such a dense cloud, $\langle\cos\theta\rangle = 0.83$ ($\theta = 34°$); and so,

$$\tau_c = \frac{1.69}{48\,(1 - 0.83 + 1.42} = 0.18 \quad .$$

The zenith cloud energy transmission, as a function of optical thickness, is presented in table 2 and figure 5 for $\langle\cos\theta\rangle = 0.83$.

From the form of equation (S-2) it cannot apply $\tau_{opt} = 0$, and the lower limit of optical thicknesses at which it does apply is still to be determined. A linear fit is provisionally adopted for $\tau_{opt} \leq 10$, so that

$$\tau_c = 1 - 0.046\,\tau_{opt} \quad , \qquad \tau_{opt} \leq 10$$
$$\langle\cos\theta\rangle = 0.83$$

This equation is evaluated in table 3, and figure 5.

---

2. EA Bucher, Computer Simulation of Light Pulse Propagation for Communication Through Thick Clouds, Appl Optics, Vol 12 (10), p 2391-2400, October 1973.
3. RE Danielson, DR Moore, and HC Van de Hulst, The Transfer of Visible Radiation Through Clouds, J Atmos Sci, Vol 26 (9), p 1078-1087, September 1969.

Table 2. Typical "thick" cloud zenith signal energy transmission ($<\cos\theta> = 0.83$).

τ_{opt}, Optical Thickness	τ_c, Energy Transmission
10	0.54
20	0.35
30	0.26
40	0.21
50	0.17
60	0.15
70	0.13
80	0.11
90	0.10
100	0.09

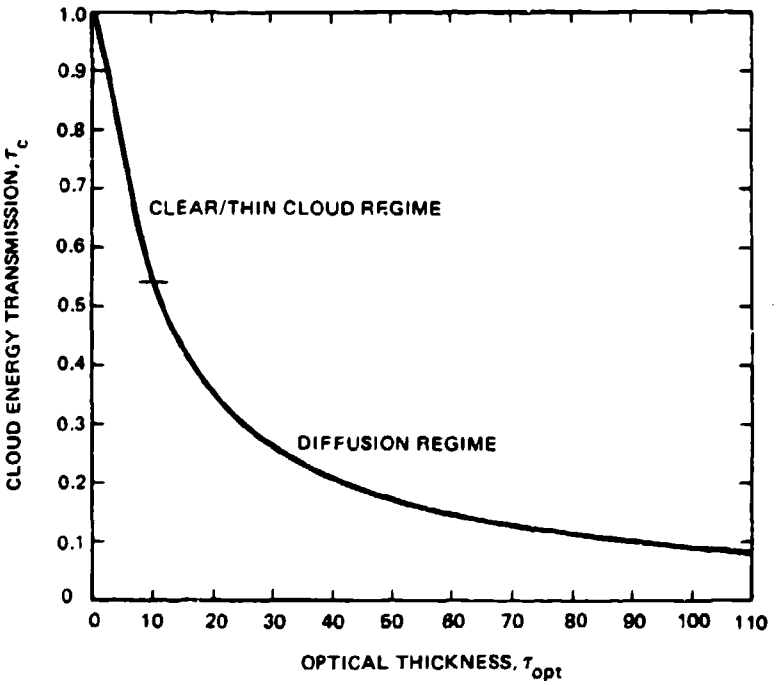

Figure 5. Thin and thick cloud energy transmission versus optical thickness for $<\cos\theta> = 0.83$.

Table 3. "Thin" cloud zenith signal energy transmission (matched to the thick cloud expression at $\tau_{opt} = 10$ for $\langle\cos\theta\rangle = 0.83$).

τ_{opt}, Optical Thickness	τ_c, Energy Transmission
0	1
2	0.91
4	0.82
6	0.72
8	0.63
10	0.54

The zenith angle dependence for thick clouds has also been modeled by Bucher and Van der Hulst (refs 2,3). It also has no experimental verification. From their tabular results, we find

$$\tau_c \propto \tau_c(o)\, A(\phi_s) \quad ,$$

when

$$A(\phi_s) = 1.69 - 0.5513\,\phi_s + 2.7173\,\phi_s^2 - 6.9866\,\phi_s^3 + 7.1446\,\phi_s^4 - 3.4249\,\phi_s^5 + 0.6155\,\phi_s^6 \quad , \qquad \text{(S-4)}$$

neglecting the effects of the "spreading out" of the beam energy with zenith angle. Since this "spreading out" may be corrected at the satellite terminal, we model it as a transmission factor,

$$(\cos\phi_s)^q \quad , \quad 0 \leq q \leq 1^{\sim} \quad .$$

The complete thick cloud signal energy transmission (including the effects of the single scatter albedo (ref 4), $\omega_0 \neq 1$) is given by:

$$\tau_c = \left\{ \frac{A(\phi_s)}{\tau_{opt}\ (1 - \langle\cos\theta\rangle) + 1.42} \right\} \left\{ 2\sqrt{3(1 - \langle\cos\theta\rangle)(1 - \omega_0)} \right\} \left\{ \tau_{opt} + \frac{1.42}{1 - \langle\cos\theta\rangle} \right\}$$

$$\times \left\{ \frac{\exp - \sqrt{3(1 - \langle\cos\theta\rangle)(1 - \omega_0)} \left\{ \tau_{opt} + \frac{1.42}{1 - \langle\cos\theta\rangle} \right\}}{1 - \exp - \left[2\sqrt{3(1 - \langle\cos\theta\rangle)(1 - \omega_0)} \left\{ \tau_{opt} + \frac{1.42}{1 - \langle\cos\theta\rangle} \right\} \right]} \right\}$$

$$\times \left[\cos\phi_s\right]^q \quad . \qquad \text{for } \tau_{opt} \geq 10 \qquad \text{(S-5a)}$$

4. The effect of $\omega_0 \neq 1$ is taken from Appendix B, equation 14, of S. Karp, "A Test Plan for Determining the Feasibility of Optical Satellite Communications Through Clouds at Visible Frequencies," NOSC TN 279, July 1, 1978.

and $0 \leq q \leq 1$, with the exact value of q dependent on the satellite optical design.

For thin clouds the diffusion, like $A(\phi_s)$ dependence, ought not to apply. Therefore, in the $\tau_{OPT} \leq 10$ regime we assume a full cosine dependence due to the extra path length in the cloud; or,

$$\tau_c = \left\{ 1 - 0.885\tau_{opt} \left[\frac{1.69}{10(1 - \langle \cos\theta \rangle) + 1.42} \right] \right\} \left[\cos\phi_s \right]^{q+1}$$

for $\tau_{opt} \leq 10$.

For

$\tau_{opt} = 0$, we use $\tau_c = \left[\cos\phi_s \right]^q$. (S-5b)

For $\phi_s \neq 0$, these models are discontinuous at $\tau_{opt} = 10$. The difference in value is about a factor of 0.58 at $\phi_s = 70$ degrees. At this stage in our knowledge of cloud propagation, we do not feel that such a factor is of prime importance and shall ignore this discrepancy until an experimentally verified model replaces it.

Table 4 and figure 6 show the zenith angle dependence of the signal energy transmission for both τ_{opt} regimes, with q = 0; i.e., satellite optics fully compensating for the zenith angle beam irradiance spread.

Table 4. Zenith angle vs signal energy transmission (normalized to $\phi_s = 0$)

ϕ_s, Signal Zenith Angle	Thick Cloud Dependence ($\tau_{opt} \geq 10$)	Thin Cloud Dependence ($\tau_{opt} \leq 10$)
0	1	1
10	0.97	0.98
20	0.96	0.94
30	0.92	0.87
40	0.86	0.77
50	0.78	0.64
60	0.69	0.5
70	0.58	0.34
80	0.44	0.17

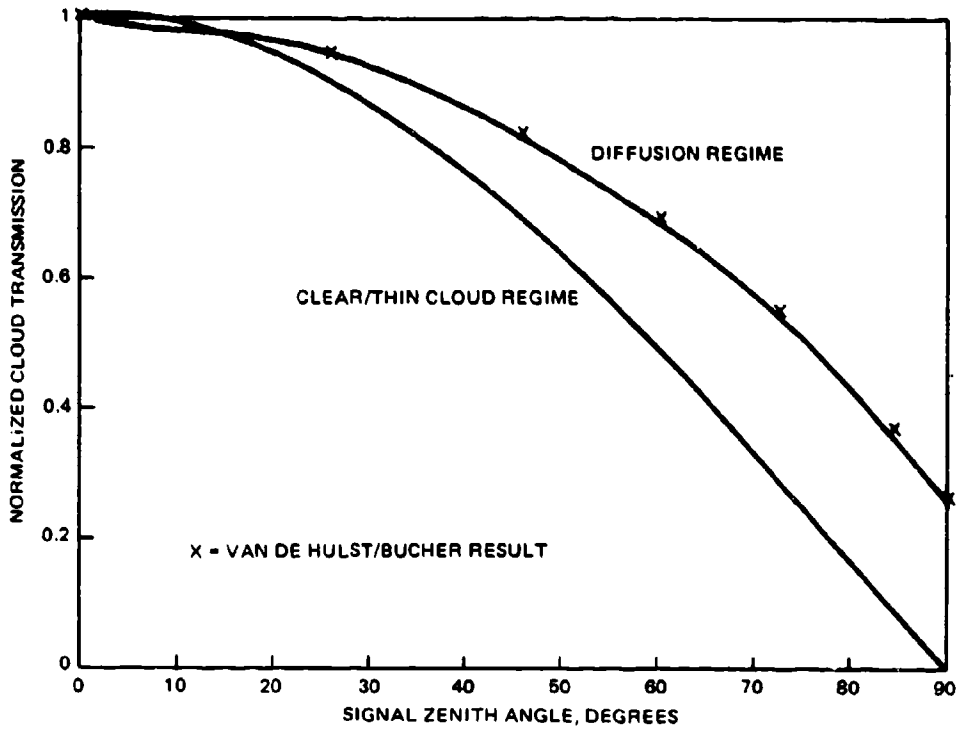

Figure 6. Thin and thick cloud zenith angle dependence of cloud transmissions normalized to zenith.

2.3.3 Cloud to Water Energy Transmission

The energy transmission of an assumed clear propagation path from the bottom of the cloud to the water surface is expressed as τ_{CW}. For large diameter emerging spots and representative clouds the energy transmission of this part of the propagation path is very high.

We consider an area element on the cloud bottom given by r dr dϕ, assuming circular symmetry and that our observation point is well away from the beam edge.

Then, assuming a thick cloud, the energy is emerging Lambationally, and taking

H = distance from cloud base to water,

R = range to satellite,

θ_T = full angle e^{-2} irradiance beamwidth (<1°); and

the beam is so large at the cloud that negligible additional in-cloud induced spreading occurs. The energy transmission is given by

$$\tau_{CW} = \frac{1}{\pi} \int_0^{2\pi} d\phi \int_0^{R\theta_T/2} r\,dr \times \left|\text{"tilt" of emitting surface area}\right| \times \left|\text{Range from surface area to water surface "receiver"}\right|^{-2} \times \left|\text{"tilt" of surface "receiver"}\right| ,$$

or

$$\tau_{CW} = \frac{1}{\pi} \int_0^{2\pi} d\phi \int_0^{R\theta_T/2} r\, dr \left\{ \frac{H}{\left[H^2 + r^2\right]^{1/2}} \right\} \left\{ \frac{1}{\left[H^2 + r^2\right]^{1/2}} \right\}^2 \left\{ \frac{H}{\left[H^2 + r^2\right]^{1/2}} \right\} ;$$

thus,

$$\boxed{\tau_{CW} = 1 - \frac{\left[H/(R\,\theta_T/2)\right]^2}{1 + \left[H/(R\,\theta_T/2\right]^2} \quad , \quad \tau_{opt} \geq 10 \quad .} \qquad \text{(S-6a)}$$

Equation (S-6a) is evaluated in table 5 and figure 7 as a function of the ratio of the cloud base height, H, to the emerging spot radius, $R\theta_T/2$.

Table 5. Thick cloud-to-water surface signal energy transmission.

$H \Big/ \frac{R\theta_T}{2}$ Cloud Base Height / Emerging Spot Radius	τ_{CW}, Energy Transmission
0	1
0.05	0.998
0.1	0.99
0.15	0.98
0.2	0.96
0.25	0.94
0.3	0.92
0.35	0.89
0.4	0.86
0.45	0.83
0.5	0.8

For typical situations, $H \Big/ \frac{R\theta_T}{2} \leq 0.2$ and so this is a very small effect for thick clouds.

For thin clouds, the net transmission is even higher for large incident beams, since the energy is not emerging isotropically, but does retain its emitted angular sense. We therefore take

$$\boxed{\tau_{CW} = 1, \text{ for } \tau_{opt} \leq 10 \quad .} \qquad \text{(S-6b)}$$

We further assume that there is no zenith angle dependence for τ_{CW} in either class.

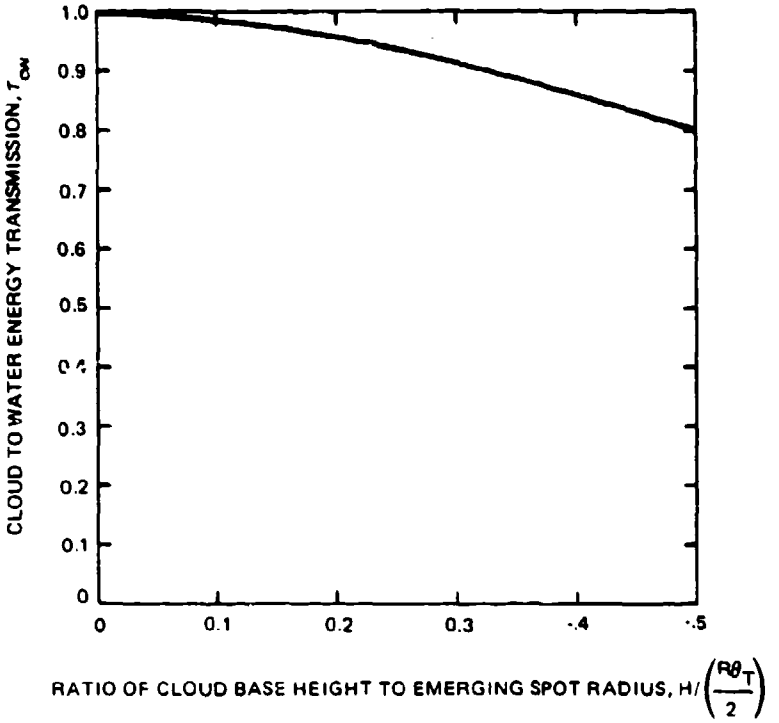

Figure 7. Thick cloud to water surface energy transmission.

2.3.4 Air-Water Interface Transmission

The signal energy transmission of the air-water interface is composed of two factors:

$$\tau_{aw} = (\tau_{aw1}) \times (\tau_{aw2}), \tag{S-7}$$

where

τ_{aw} = total energy transmission of air-water interface, with

τ_{aw1} = air-water interface transmission due to index of refraction discontinuity; and

τ_{aw2} = air-water interface transmission due to foam and streaks on the sea surface.

This section treats τ_{aw1} while τ_{aw2} is discussed in section 2.3.6.

For thin clouds and clear weather ($\tau_{opt} \leq 10$), we assume the signal beam retains its angular sense. Gordon (ref 5) has estimated the value of τ_{aw1} as a function of surface wind speed and signal zenith angle, for the Cox and Munck (ref 6) wave slope distribution, as shown in table 6 and figure 8.

For thick clouds ($\tau_{opt} > 10$), the energy is modelled as being incident on the sea surface from the entire hemisphere. Using the Fresnel refraction equation, and neglecting wave effects, we find

5. J Gordon, Directional Radiance (Luminescence) of the Sea Surface, S10, ref 89-20, October 1969.
6. C Cox and W Munck, Statistics of the Sea Surface Derived from Sun Glitter, J Marine Res, Vol 13 2, 1954.

Table 6. τ_{aw} Time-averaged downlink air-sea interface transmittance (for thin clouds, $\tau_{opt} \leq 10$).

ϕ_s Signal Zenith Angle in Air	v, Wind Speed								
	0	1.03	2.06	4.12	7.21	10.3	13.4	16.5	19.6 m/sec
	0	2	4	8	14	20	26	32	38 knots
0	0.979	0.977	0.976	0.974	0.970	0.967	0.963	0.960	0.956
5	0.975	0.974	0.972	0.970	0.966	0.963	0.959	0.956	0.952
10	0.964	0.962	0.961	0.959	0.955	0.951	0.948	0.944	0.941
15	0.945	0.944	0.943	0.940	0.936	0.933	0.929	0.926	0.922
20	0.920	0.918	0.917	0.914	0.910	0.907	0.903	0.899	0.896
25	0.887	0.885	0.884	0.881	0.877	0.873	0.870	0.866	0.863
30	0.847	0.845	0.844	0.841	0.837	0.833	0.829	0.826	0.822
35	0.800	0.798	0.797	0.794	0.790	0.786	0.782	0.779	0.775
40	0.747	0.745	0.743	0.741	0.736	0.733	0.729	0.725	0.722
45	0.687	0.685	0.684	0.681	0.677	0.673	0.669	0.666	0.663
50	0.620	0.619	0.617	0.615	0.611	0.608	0.605	0.602	0.599
55	0.548	0.546	0.545	0.543	0.540	0.538	0.536	0.534	0.532
60	[illegible]	0.468	0.468	0.466	0.465	0.464	0.464	0.464	0.463
65	[illegible]	0.385	0.385	0.386	0.387	0.389	0.391	0.393	0.395
70	0.295	0.298	0.299	0.303	0.310	0.315	0.321	0.325	0.329
75	0.203	0.209	0.214	0.244	0.236	0.247	0.255	0.262	0.268
80	0.113	0.126	0.136	0.153	0.172	0.186	0.197	0.206	0.213
85	0.0361	0.0610	0.0751	0.0969	0.119	0.135	0.148	0.157	0.165
90	0	0.0265	0.0390	0.0594	0.0809	0.0961	0.108	0.117	0.124

$$\tau_{aw1} = 1 - \int_0^{\pi/2} R(\phi_s) \sin \phi_s \, d\phi_s \quad , \tag{S-8}$$

for ϕ_s = signal zenith angle,

$R(\phi_s)$ = Sea Surface reflectance as a function of zenith angle.

Also,

$$R(\phi_s) = \frac{[f_1(\phi_s) - f_2(\phi_s)]\, f_3(\phi_s)}{[f_1(\phi_s) + f_2(\phi_s)]\, [f_3(\phi_s) + f_2(\phi_s)]} \quad , \tag{S-9a}$$

for

$$f_1(\phi_s) = \sin^2(\phi_s) \left| n^2 + \cos 2\phi_s \right| \quad , \tag{S-9b}$$

$$f_2(\phi_s) = \sin \phi_s \sin 2\phi_s \left| n^2 - \sin^2 \phi_s \right|^{1/2} \quad , \tag{S-9c}$$

$$f_3(\phi_s) = n^2 \cos^2 \phi_s - \sin^2 \phi_s \cos 2\phi_s, \text{ and} \tag{S-9d}$$

n = sea-water index of refraction.

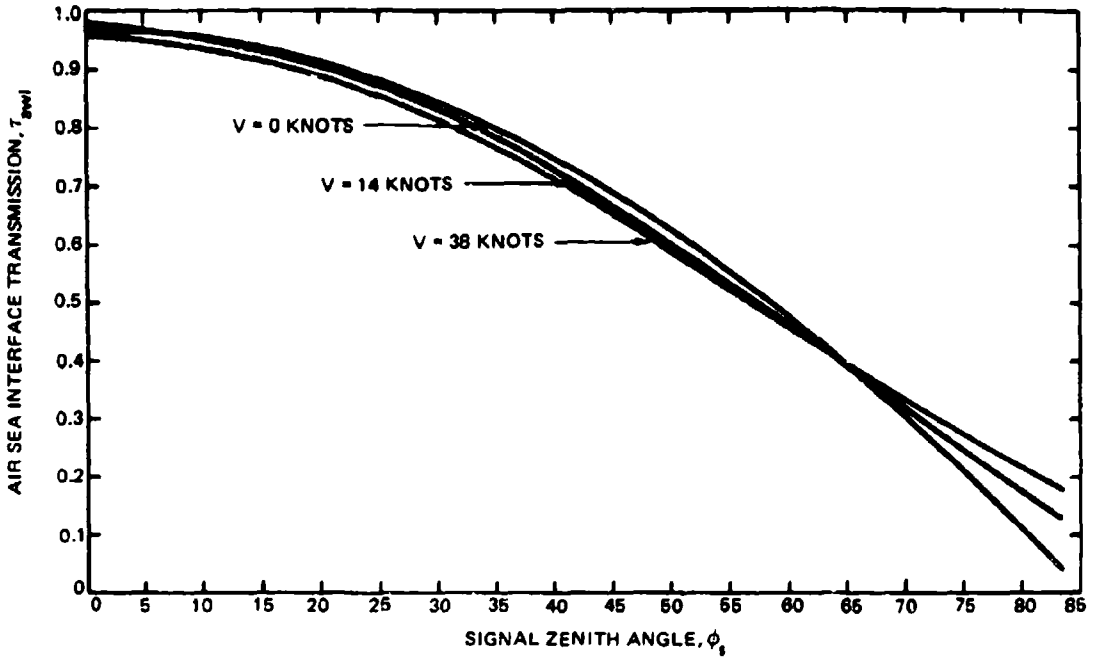

Figure 8. Thin cloud air-sea interface transmission as a function of signal zenith angle (ϕ_s) and surface wind speed, v .

Using n = 1.33, equation (S-7) has been evaluated with the result:

$$\tau_{awl} = 0.83, \tau_{opt} \geq 10 \quad . \tag{S-10}$$

Equation (S-10) is an approximation, since it has neglected the wave structure of the surface and is discontinuous with the $\tau_{opt} < 10$ values in table 6. It will be used pending further analysis and experimentation.

There is no zenith angle dependence for thick clouds for τ_{awl}.

2.3.5 Air-Water Angular Effects

The wave slopes on the sea surface will cause an overall increase in the beam divergence of an incident beam. However, for the propagation path considered here, this will only have an effect for thin cloud and clear weather cases ($\tau_{opt} < 10$).

We describe the statistical effects of the surface by $\Delta\theta_{AW}$ = half-angle of the rms additional beam divergence of the radiance profile. Adopting Karp's unverified model (ref 7) we use the expression,

$$\Delta\theta_{AW} = 0.0103\ v^{1/2}, \tau_{opt} < 10, \tag{S-11a}$$

7. NELC TR 2021, Submarine-Aircraft and Submarine-Satellite Optical Communications Systems Model (U), RE Howarth, ME Hyde, and WR Stone, Confidential, 1977.

for v = surface wind speed in knots, and the index of refraction of sea water has been taken = 4/3. Equation (S-11a) is evaluated in table 7 and figure 9 for v in knots (and m/sec) and $\Delta\theta_{AW}$ in radians (and degrees).

The relative contribution of $\Delta\theta_{AW}$ to the distribution of radiance at the receiver will be discussed in section 2.3.8. Except for the clearest water, this has a small effect; and so the impact of neglecting zenith angle effects and dissimilar wave slopes in the downwind and crosswind direction may be negligible. We therefore adopt this model, and

$$\Delta\theta_{AW} = 0, \tau_{opt} \geq 10, \qquad \text{(S-11b)}$$

until better information is available.

Table 7. Half-angle rms air-water interface effects

v, Wind Speed		$\Delta\theta_{AW}$	
Knots	Metres/Sec	Milliradians	Degrees
0	0	0	0
2	1.03	14.6	0.84
4	2.06	20.7	1.18
8	4.12	29.2	1.67
14	7.21	38.6	2.21
20	10.3	46.2	2.65
26	13.4	52.6	3.0
32	16.5	58.4	3.35
38	19.6	63.6	3.64

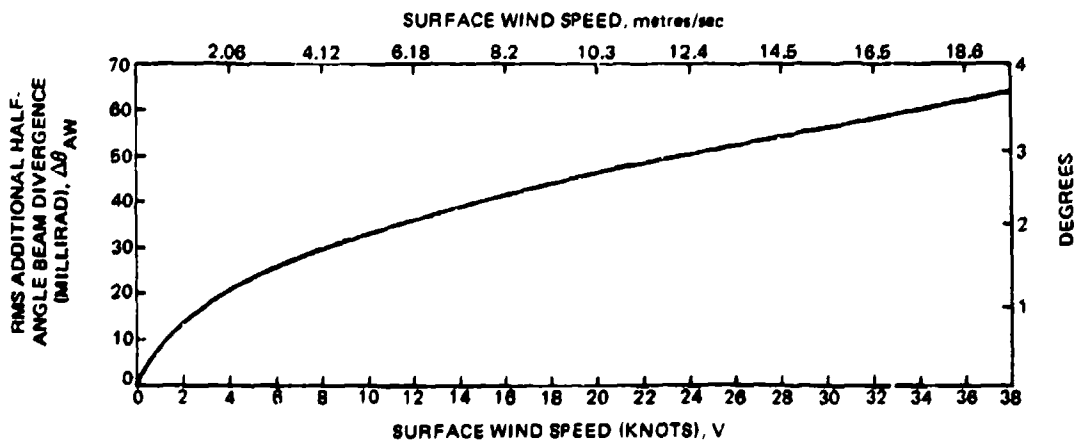

Figure 9. Half-angle rms air-water interface effects as a function of wind speed v.

2.3.6 Relative Surface Foam Coverage

The energy transmission of the air-water interface is composed of the factors:

$\tau_{aw} = (\tau_{aw1}) \times (\tau_{aw2})$, with

τ_{aw} = total energy transmission of the sir-water interface, where

τ_{aw1} = air-water interface transmission due to index of refraction discontinuity

and

τ_{aw2} = air-water interface transmission due tc foam and streaks on the water surface.

This section treats τ_{aw2}, while τ_{aw1} was discussed in section 2.3.4. Independent of the cloud conditions, a model relating the fraction of surface covered to the surface wind speed is given by (ref 8):

$$C_f = (1.2 \times 10^{-5})\, v^{3.3},\ v \leq 9\text{m/sec, and} \qquad \text{(S-12)}$$

$$C_f = (1.2\,(10^{-5})\, v^{3.3}\,(0.225\, v - 0.99),\ v \geq 9\text{m/sec;} \qquad \text{(S-13)}$$

where,

C_f = fraction of surface covered, and

v = surface wind speed in metres/sec.

Assuming the foam and streaks have an albedo of 1, the value of τ_{aw2} is given by:

$$\tau_{aw2} = 1 - (1.2\,(10^{-5}))\, v^{3.3},\ v \leq 9\text{m/sec, and} \qquad \text{(S-14a)}$$

$$\tau_{aw2} = 1 - (1.2\,(10^{-5}))\, v^{3.3}\,(0.225v - 0.99);\ v \geq 9\text{m/sec} \qquad \text{(S-14b)}$$

Equations (S-14a, b) are evaluated in table 8 and figure 10 for V in metres/sec (and knots). Although this model neglects zenith angle effects, it is adopted pending further experimental work.

2.3.7 Water Energy Transmission

The energy transmission of the water portion of the propagation path is denoted by τ_w. For most water types and receiver depths, the dominant cause of attenuation is the diffuse attenuation coefficient (ref 8) of the water, k. We therefore use the model:

$$\boxed{\tau_w = \exp\,[-(k \times (\text{path length in water})]}. \qquad \text{(S-15a)}$$

The path length in the water is given by:

$D/\cos(\phi_s^w)$,

8. HR Gordon and MM Jacobs, Albedo of the Ocean-Atmospheric System: Influence of the Sea Foam, Appl Optics, Vol 16 (8), p 2257-2260, August 1977.

Table 8. Air-water energy transmission due to surface foam and streaks (assuming a foam/streak albedo = 1).

v, Wind Speed		
Knots	Metres/Sec	τ_{aw2}
0	0	1
2	1.03	1
4	2.06	1
8	4.12	1
14	7.21	0.99
20	10.3	0.96
26	13.4	0.87
32	16.5	0.66
38	19.6	0.25

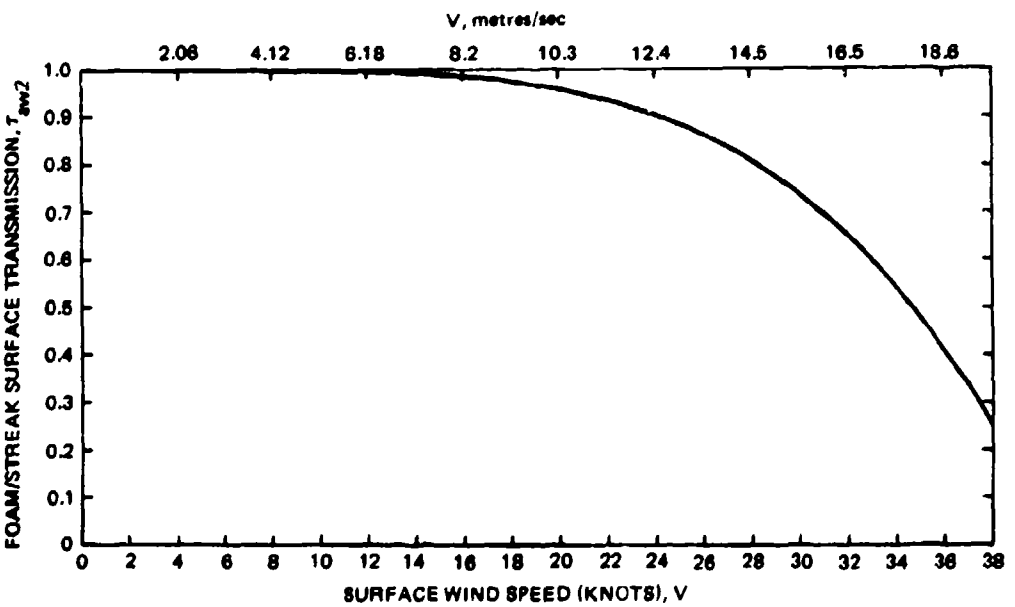

Figure 10. Foam/streak surface coverage transmission versus surface wind speed.

where

D = receiver depth, and

ϕ_s^w = in-water signal zenith angle.

From Snell's law,

$$n \sin(\phi_s^w) = \sin \phi_s \quad ,$$

where

n = water index of refraction, and

ϕ_s = in-air signal zenith angle.

Table 9 and figure 11 show the values of equation (S-15) for n = 1.33. Since many areas of the ocean have a layered structure for k, we modify our basic equation to yield

$$\frac{k\,D}{\cos(\phi_s^w)} = \frac{1}{\cos(\phi_s^w)} \sum_{i=1}^{j} (k_i D_i) \quad ,$$

where we have assumed there are j layers which differ in their k values, but not in their indices of refraction. Therefore, the adopted model is:

$$\tau_w = \exp - \left\{ \frac{\sum_{i=1}^{j} k_i D_i}{\cos \phi_s^w} \right\} \quad , \text{for} \qquad \text{(S-15b)}$$

$$\phi_s^w = \sin^{-1} \frac{1}{n} \sin \phi_s \quad \text{and} \quad \sum_{i=1}^{j} D_i = D$$

This model is uncertain in many ways:

(1) the value of k_i to use,

(2) the values of D_i, and

(3) its applicability in very clear water and/or at shallow receiver depths.

Consequently, although it is the best model available, it should be revised when better information becomes available.

2.3.8 Water Distribution of Radiance

There is no experimentally verified expression for the in-water distribution of signal radiance, as a function of incident beam collimation, incident beam zenith angle, water properties, and receiver depth. Any model expression must take into account the following items:

Table 9. Relation between in-air and in-water signal zenith angles (assuming sea-water index of refraction, n = 1.33)

ϕ_s, In-Air Signal Zenith Angle (degrees)	ϕ_s^w, In-Water Signal Zenith Angle (degrees)
0	0
5	3.75
10	7.48
15	11.19
20	14.86
25	18.48
30	22.02
35	25.48
40	28.82
45	32.03
50	35.07
55	37.91
60	40.51
65	42.82
70	44.81
75	46.42
80	47.61
85	48.34

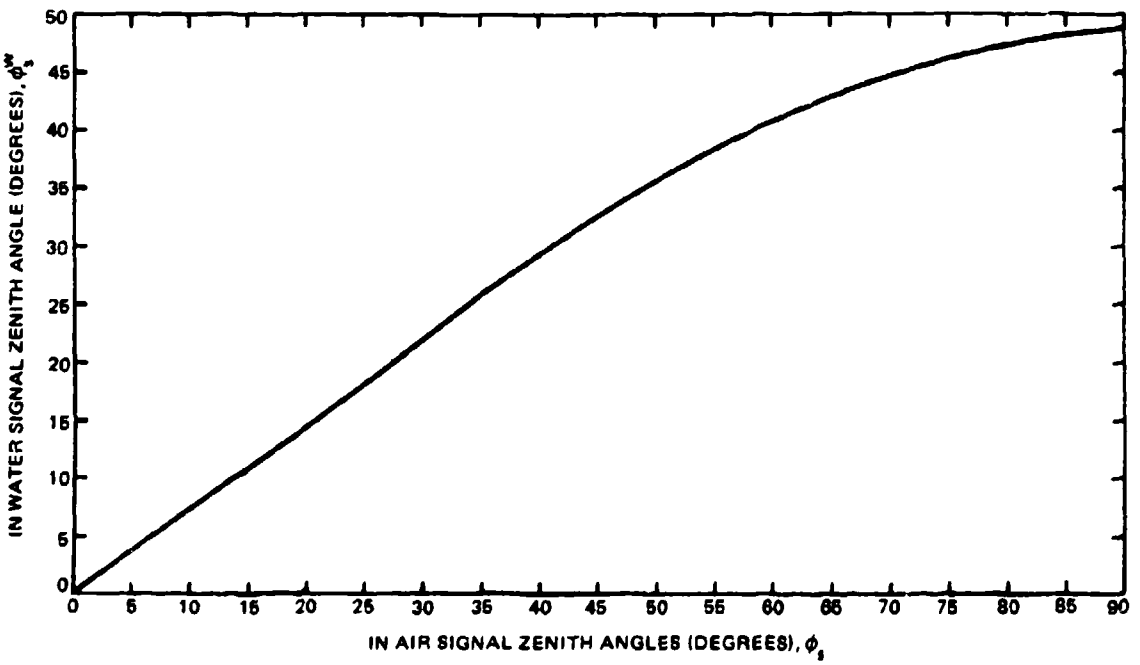

Figure 11. Relation between in-air and in-water signal zenith angles (assuming sea-water index of refraction, n = 1.33).

(1) the in-air zenith angle of the signal,

(2) the radiance distribution incident on the water,

(3) the air-water interface effects,

(4) the in-water zenith angle of the signal,

(5) the in-water scattering effects, and

(6) the in-water absorption effects.

In considering these last two, we note that the energy should decrease away from zenith due to absorption, depending on depth and the water properties. We have therefore considered the following zenith angle dependencies for the radiance at the submarine receiver:

(1) Uniform,

(2) $1 - \left(\frac{\phi^w}{\phi_0}\right)$

(3) $\frac{\sin\left(\phi_0 - \phi^w\right)}{\sin \phi_0}$

(4) $1 - \left[\frac{\sin(\phi^w)}{\sin(\phi_0)}\right]^2$

(5) $\exp\left[-\left(\frac{\phi^w}{\phi_0}\right)^2\right]$.

Moreover,

ϕ^w = angle measured from the axis, or principal ray direction, of the in-water signal radiance;

and

ϕ_0 = angle at which the signal radiance reaches a benchmark.

We adopt (4), $1 - \left[\frac{\sin \phi^w}{\sin \phi_0}\right]^2$, because it is easy to work with and appears to give a reasonable representation of the assumed radiance.

ϕ_0 is related to the half-power point of the received radiance by the equation:

$$\frac{1}{2} = \frac{1 - \cos(\phi_{1/2}) - \frac{1}{3\sin^2 \Phi_0}\left[\cos \phi_{1/2} \sin^2 \phi_{1/2} + 2\cos \phi_{1/2} - 2\right]}{1 - \cos \phi_0 - \frac{1}{3\sin^2 \phi_0}\left[\cos \phi_0 \sin^2 \phi_0 + 2\cos \phi_0 - 2\right]} \qquad \text{(S-16a)}$$

Equation (S-16a) is evaluated in table 10. Values between those shown are obtained by linear interpolation.

Table 10. Relation of radiance zero point, ϕ_0, and received radiance half-power point, $\phi_{1/2}$, for $1 - (\sin \phi^w / \sin \phi_0)^2$ radiance distribution

$\phi_{1/2}$ (degrees)	ϕ_0 (degrees)
3.8	5
7.6	10
11.4	15
15.2	20
19.0	25
22.7	30
26.5	35
30.2	40
33.9	45
37.5	50
41.1	55
44.6	60
48.1	65
51.6	70
54.9	75
58.2	80

We adopt the NOSC developed expression for the half-power point in terms of incident beam divergence, air-water angular effects and in-water scattering effects, and add them up as if they were three statistically* independent effects:

$$\phi_{1/2} = \left[f_w + f_{aw} + f_a \right]^{1/2} , \qquad \text{(S-16b)}$$

for

$$f_w = \text{water contribution} = \frac{\phi_{si}^2 \, s \, D}{\cos \phi_s^w} \quad , \text{all } \tau_{opt} ; \qquad \text{(S-17a)}$$

*This is actually an empirical result, and appears to fit the NOSC experimental results. A completely consistent theory of all these effects would not use the statistical independence as the justification for this expression.

$$f_{aw} = (0.0103\, V^{1/2})^2 \quad \text{for } \tau_{opt} < 10 \qquad \text{(S-17b)}$$

$$= 0 \qquad \text{for } \tau_{opt} \geq 10 \quad ; \qquad \text{(S-17c)}$$

and

$$f_a = \left(\frac{1}{n}\right)^2 (0.294\, \theta_T)^2 \text{ for } \tau_{opt} < 10 \qquad \text{(S-17d)}$$

$$= (33.8°)^2 \qquad \text{for } \tau_{opt} \geq 10 \; . \qquad \text{(S-17e)}$$

Here,

θ_{si}^2 = mean square single scattering angle in water,

s = scattering coefficient in water,

D = receiver depth,

ϕ_s^w = in-water signal zenith angle,

v = surface wind speed in knots,

τ_{opt} = cloud optical thickness,

n = water index of refraction, and

θ_T = e^{-2} irradiance full angle of in-air incident beam.

Equation (S-17a) is the NOSC (ref. 7) expression, and contains the only zenith angle dependence for the radiance distribution. We could modify it for layering effects; $\theta_{s1} \rightarrow \theta_{s1i}$; $s \rightarrow s_i$; $D \rightarrow D_i$ and $f_w \rightarrow \sum_i (f_{wi})$, but shall not at this time, until further experimental results are obtained.

Equations (S-17b) and (S-17c) are based on the discussion in section 2.3.5.

Equation (S-17d) is the refraction-corrected beam divergence of the collimated incident beam, again assuming a Gaussian distribution in angle.

Equation (S-17e) assumes that, after penetration through thick clouds, the light has a uniform angular distribution at the water surface. Then, Snell's law implies that, just below the water surface, all the energy is contained within a solid angle of half-angle = 48.6 degrees, neglecting wave action. Then, defining the half-power angle as the half-angle of the solid angle containing half of the energy, implies

$1 - \cos \phi = \frac{1}{2}$ (1 - cos 48.6 degrees), or

ϕ = 33.8 degrees.

The radiance distribution enters into the expression for the received energy by the expression

$$f(\theta_R, \phi_0, \delta) = \frac{\int_{\Omega_R} \left[1 - \left(\frac{\sin \phi^w}{\sin \Phi_0}\right)^2\right] d\Omega}{\int_{\Omega_0} \left[1 - \left(\frac{\sin \phi^w}{\sin \phi_0}\right)^2\right] d\Omega} \quad ;$$

where,

Ω_R = solid angle of the receiver,

Ω_0 = full solid angle which all the energy is within,

θ_R = half-angle of the receiver field of view, and

δ = off-set angle between receiver optical axis and axis of the incoming light.

Therefore, for the general case,

$$f(\theta_R, \phi_0, \delta) = \frac{\int_0^{2\pi} d\theta \int_0^{\theta_R} d\phi^{w} \sin \phi^w \left[1 - \left(\frac{\sin \phi^{w'}}{\sin \phi_0}\right)^2\right]}{\int_0^{2\pi} d\theta \int_0^{\phi_0} d\phi^{w} \sin \phi^w \left[1 - \left(\frac{\sin \phi^w}{\sin \phi_0}\right)^2\right]} \qquad \text{(S-18a)}$$

for

$$\phi^{w'} = \cos^{-1} \left\{ \cos \phi^w \cos \delta + \sin \phi^w \sin \delta \sin \theta \right\} \quad .$$

For perfect alignment between the received light axis and the receiver ($\delta \to 0$), the integral can be analytically evaluated, with the result

$$f(\theta_R, \phi_0) = \frac{1 - \cos \theta_R - \frac{1}{3 \sin^2 \theta_0} \left[\cos \theta_R \sin^2 \theta_R + 2 \cos \theta_R - 2\right]}{1 - \cos \theta_0 - \frac{1}{3 \sin^2 \theta_0} \left[\cos \phi_0 \sin^2 + 2 \cos \phi_0 - 2\right]} \qquad \text{(S-18b)}$$

Equation (S-20b) has been evaluated in figures 12, 13 for $\phi_0 = 30$ degrees (figure 12) and $\phi_0 = 70$ degrees (figure 13) and $\delta = 0$, 20, 30, 40, 50, and 60 degrees.

These results will be used in section 2.3.10.

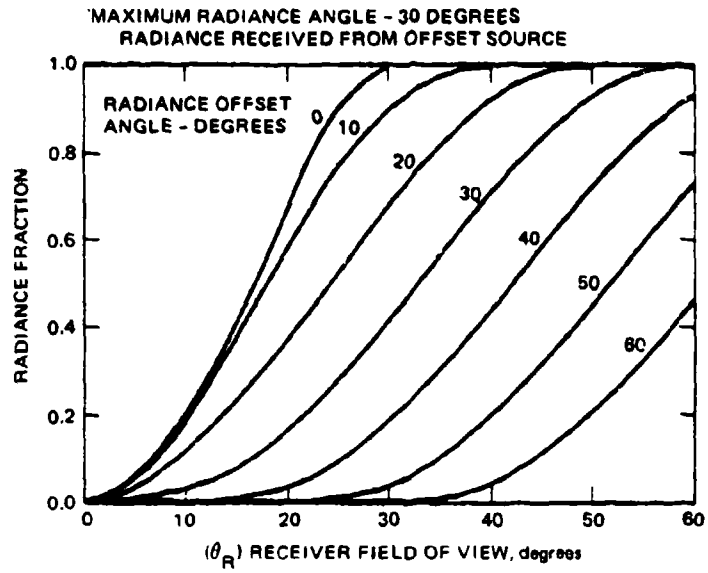

Figure 12. $f(\theta_R, \phi_0, \delta)$ for $\phi_0 = 30°$.

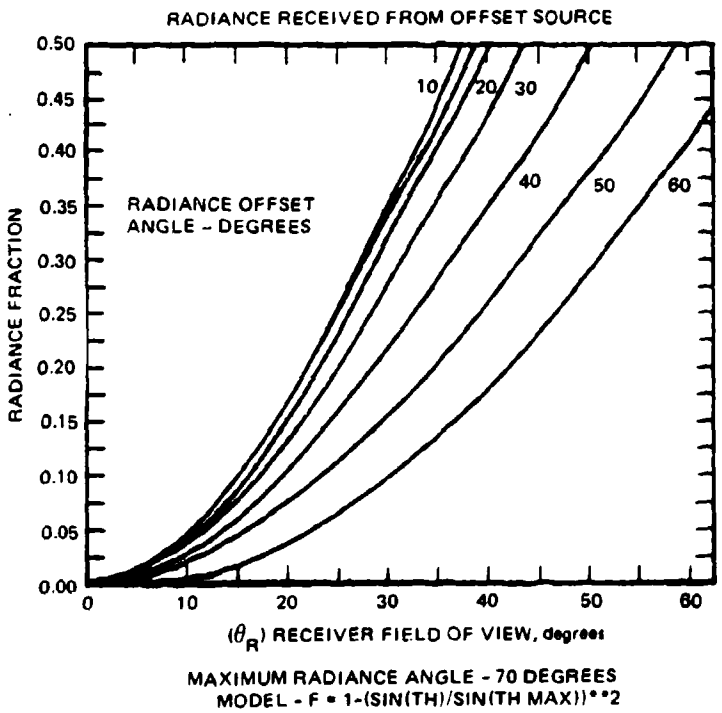

Figure 13. $f(\theta_R, \phi_0, \delta)$ for $\phi_0 = 70°$.

2.3.9 Received Pulse Width/Shape

There is no verified model which predicts the received pulse width and shape at the submarine receiver as a function of cloud properties, cloud height above the water, water properties, and the receiver field-of-view. It is not intended to develop such a final model now, but only to present some reasonable expressions needed for the provisional model here.

It is the universal experience of experimenters (both empirical and computer simulation) that after penetration of a multiple scattering medium, the received pulse has a short rise time and a long falltime. Because of its nearness to Bucher's computer simulations (ref. 2, as shown in figure 14) we shall assume the underwater receiver sees a pulse shape given by:

$$f(t) = te^{-kt} \quad . \tag{S-19a}$$

The properties of this form are as follows:

$$\text{maximum value of } f(t) \text{ occurs at } t_m = \frac{1}{k} \quad , \tag{S-19b}$$

$$\text{maximum value of } f(t) = t_m e^{-1} = 0.368\, t_m, \text{ with} \tag{S-19c}$$

average value of t, defined as

$$\left\{ \frac{\int_0^\infty t\, f(t)\, dt}{\int_0^\infty f(t)\, d\, t} \right\} = 2\, t_m \quad . \tag{S-20a}$$

Half-power points of f(t) occur at $0.233\, t_m$ and $2.68\, t_m$, so the width between half-power points $= 2.45\, t_m$: (S-20b)

The rms value of t, defined as

$$\left\{ \frac{\int_0^\infty t^2\, f(t)\, d\, t}{\int_0^\infty f(t)\, d\, t} \right\}^{1/2} = \sqrt{6}\, t_m \quad . \tag{S-20c}$$

Hence, the variance of t is given by

$$\text{var } t = (\overline{t^2} - \bar{t}^2) = 2\, t_m^2 \quad , \tag{S-21a}$$

and its standard deviation, by

$$[\overline{t^2} - \bar{t}^2]^{1/2} = \sqrt{2}\, t_m \quad . \tag{S-21b}$$

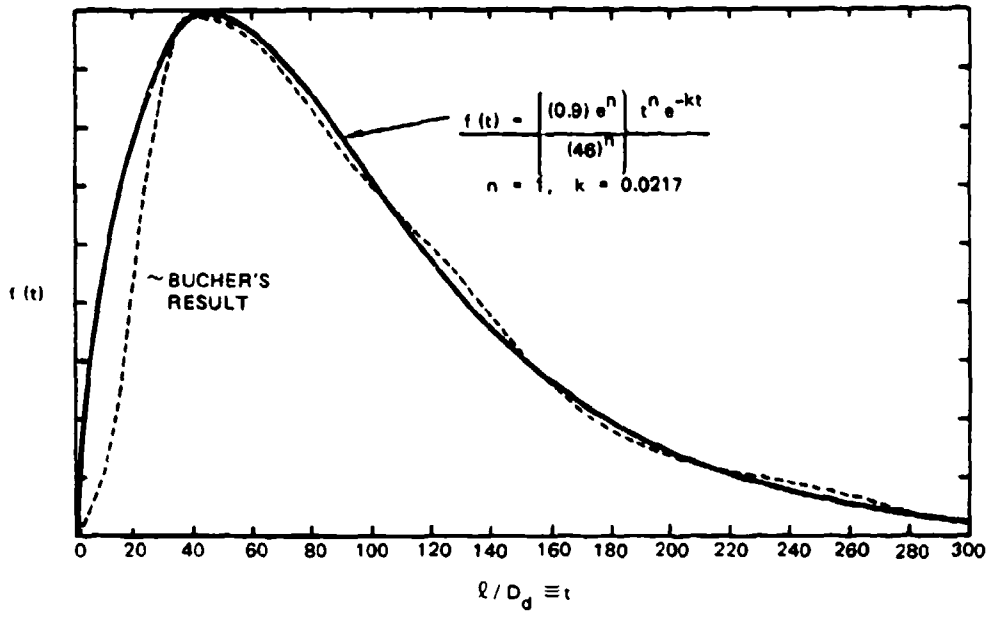

Figure 14. Comparison of f(t) and Bucher's Monte Carlo pulse shape.

The area under the f(t) curve is given by

$$\int_0^\infty f(t)\, d\, t = t_m^2 \quad . \tag{S-22}$$

In principle, there are three significant contributions to the received pulse width, which we shall define as the time between half-power points,

$$2.45\, t_m = (\Delta t_c + \Delta t_{cw} + \Delta t_w) \quad , \tag{S-23}$$

where we have neglected the initial pulse width at the transmitter, assumed that the effects add serially, not statistically, and where

Δt_w = pulse width due to water portion of the path,

Δt_{cw} = additional pulse width due to cloud-to-water path, and

Δt_c = pulse width after emerging from the cloud.

The additional pulse width due to the water portion of the path is caused by the in-water multiple scattering, and so it occurs in the absence or presence of clouds. As seen in figure 15, a signal at a zenith angle of 0 degrees and a receiver of half-angle θ_R at a depth D leads to a pulse width (for a uniform contribution throughout that field of view), of

$$\Delta t_w < \frac{D}{c/n} \left\{ \frac{1 - \cos \theta_R}{\cos \theta_R} \right\} \quad , \text{all } \tau_{opt} \tag{S-24}$$

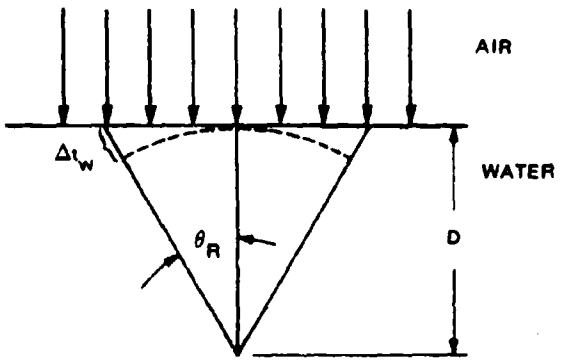

Figure 15. In-water pulse width calculation geometry.

for

c = speed of light and

n = water index of refraction.

When the signal zenith angle is not 0 degrees, an additional pulse stretching occurs, as shown in figure 16. The effect is given by

$$\Delta t_{cw} \leq \frac{2\,D \tan \theta_R \sin \phi_s}{c} \quad , \text{for } \tau_{opt} \leq 10 \qquad \text{(S-25a)}$$

where ϕ_s = signal zenith angle. When thick clouds are in the path, there is no single zenith angle defined below the clouds and so this expression will not apply.

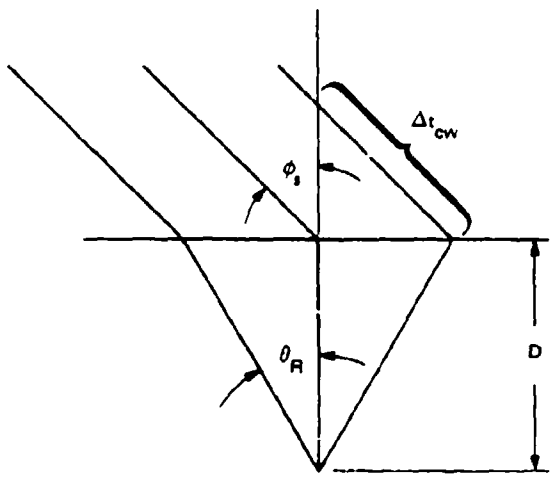

Figure 16. Signal zenith angle induced additional pulse stretching.

For thin clouds ($\tau_{opt} \leq 10$) we have found no verified expression for the cloud effects or the cloud to water effects. Since equations (S-28) and (S-29) already imply stretching to a few hundred nanoseconds, we can neglect the thin cloud effects, and take

$$\Delta t_c = 0, \text{ for } \tau_{opt} \leq 10 \quad . \qquad \text{(S-26a)}$$

(All zenith angles.)

For thick clouds we adopt the Stotts (ref. 9) expression, so that:

$$\Delta t_c = \frac{T}{c} \left\{ \frac{0.3}{\omega_o \tau_{opt} \theta^2} \left[(1 + 2.25\, \omega_o \tau_{opt} \theta^2)^{1.5} - 1 \right] - 1 \right\} , \qquad \text{(S-26b)}$$

for $\tau_{opt} \geq 10$.

(All zenith angles.)

where,

c = speed of light in air

T = cloud geometrical thickness,

ω_o = single scatter albedo, and

θ = mean scattering angle in the cloud.

Equation (S-26b) has been evaluated in table 11 and figure 17 for the typical values of $\omega_o \approx 1$, $\theta = 0.66$ rad (37 degrees), and fixing $T = \tau_{opt}/\sigma_c = 25\, \tau_{opt}$ suitable for a stratocumulus cloud. (Also shown for comparison, is the result estimated in ref 2.)

These values probably overestimate the pulse widths at the lower values of τ_{opt}, but they are adopted until a verified model for all vaues of τ_{opt} is developed.

We use the values from table 11 for $\tau_{opt} = 20$, 40, and 60 along with the normalized pulse shape $[\bar{f}(t) = (t_m^{-2})\, t \exp - (t/t_m)]$, to plot representative pulses in figure 18. The drastic dependence of the pulse height and width on optical thickness for the assumed model is clearly seen.

A careful analysis of the thick cloud to water propagation region has found that it adds a negligible amount relative to Δt_c for reasonable cloud properties and cloud heights. Hence, we take

$$\Delta t_{cw} = 0, \text{ for } \tau_{opt} \geq 10 \quad . \qquad \text{(S-25b)}$$

(All zenith angles.)

We therefore have adopted a complete model for all effects and all optical thicknesses. It shall be used further in the next section.

9. LB Stotts, Closed Form Expression for Optical Pulse Broadening in Multiple Scattering Media, Appl Optics, Vol 17 (4), p 504-505, 15 February 1978.

Table 11. Typical "thick" cloud pulse broadening for $\omega_o = 1$, $\theta = 37°$ and $\sigma_c = 0.04\ m^{-1}$.

τ_{opt}, Optical Thickness	T, Geometrical Thickness (km)	Δt_c, Pulse Width (μsec)
10	0.25	1.15
20	0.5	3.65
30	0.75	7.08
40	1.0	11.27
50	1.25	16.13
60	1.5	21.55
70	1.75	27.48
80	2.0	33.93
90	2.25	40.88
100	2.5	48.25

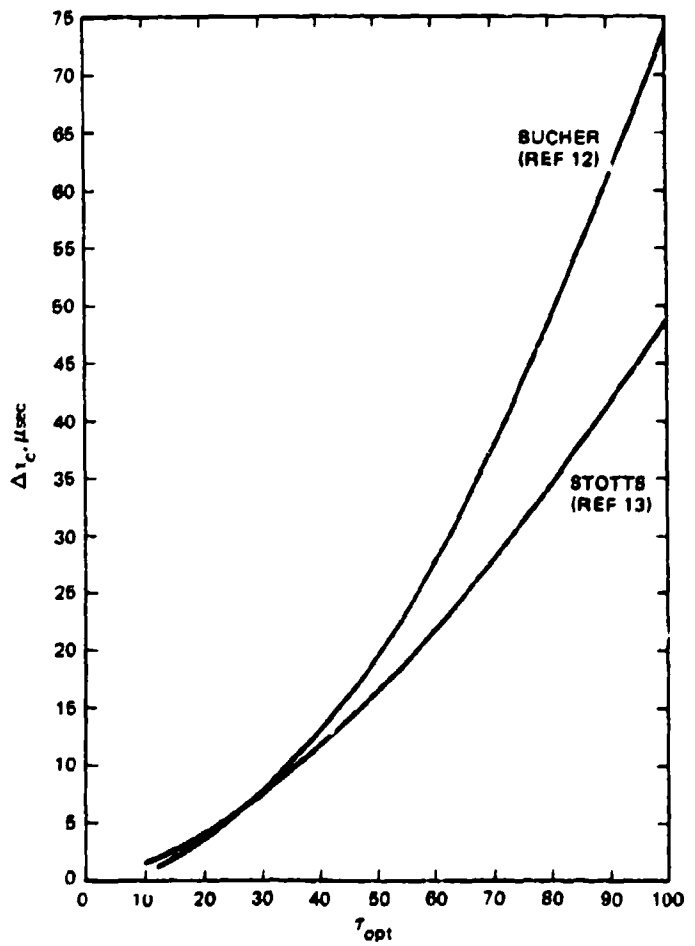

Figure 17. Cloud induced pulse stretching as a function of optical thickness ($\sigma_c = 0.04\ m^{-1}$).

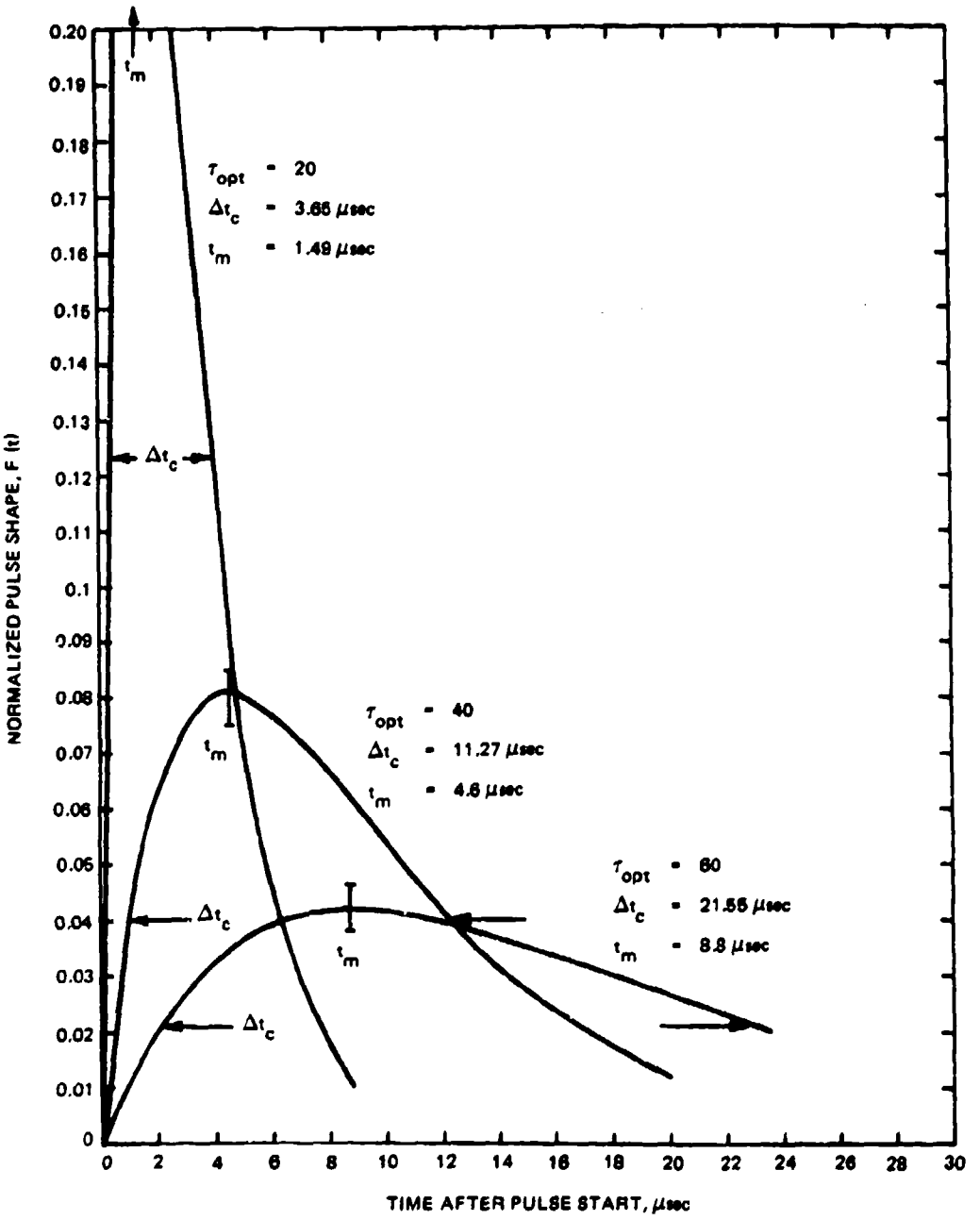

Figure 18. Representative normalized pulse shapes as a function of cloud optical thickness.

2.3.10 Overall Signal Equations

The optical detection mechanism responds to the received energy as a function of time, i.e., the instantaneous optical power. The total received optical energy and the instantaneous optical power are related by:

$$E_R = \int_o^\infty P_R(t)\, dt \qquad \text{(S-27)}$$

for

E_R = total received optical energy per pulse, and

$P_R(t)$ = instantaneous received optical power.

Writing

$$P_R(t) = A_E\, f(t), \qquad \text{(S-28)}$$

for

A_E = normalization parameter, and

$f(t)$ = received optical pulse shape,

then

$$A_E = \frac{E_R}{\int_o^\infty f(t)\, dt}\ , \qquad \text{(S-29)}$$

so that

$$P_R(t) = \frac{E_R\, f(t)}{\int_o^\infty f(t)\, dt}\ . \qquad \text{(S-30)}$$

Using the received pulse shape of section 2.3.9,

$$f(t) = t \exp - \frac{t}{t_m}\ , \qquad \text{(S-31)}$$

$$\int_o^\infty f(t)\, dt = t_m^2 \qquad \text{(S-32)}$$

and

$$P_R(t) = E_R \left| \frac{\exp - (t/t_m)}{t_m^2} \right| \ ; \qquad \text{(S-33)}$$

for

$$t_m = (2.45)^{-1} \times \text{(time between half power points)}. \tag{S-34}$$

The total received optical energy is given by the range equation:

$$\begin{aligned} E_R = {} & \text{(transmitted energy per pulse)} \times \text{(transmitter optics transmission)} \\ & \times \left(\frac{\text{solid angle subtended by the receiver at the source}}{\text{solid angle transmitted into}} \right) \\ & \times \text{(clear atmospheric energy transmission)} \\ & \quad \times \text{(cloud energy transmission)} \\ & \times \text{(cloud to water energy transmission)} \\ & \times \text{(air-water interface energy transmission)} \\ & \quad \times \text{(water energy transmission)} \\ & \times \text{(receiver optics transmission)} \\ & \times \text{(fraction of incident radiance within receiver field-of-view)}. \end{aligned} \tag{S-35}$$

We take

E_p = transmitted energy per pulse,

γ_T = transmitter optics transmission,

γ_R = receiver optics transmission,

d = diameter of receiver aperture,

R = range from source to receiver,

$\frac{(\pi d^2/4)}{R^2}$ = solid angle subtended by the receiver at the source,

θ_T = full angle e^{-2} irradiance angle transmitted into*,

$\frac{\pi \theta^2_T}{4}$ = solid angle transmitted into,

τ_a = clear atmosphere energy transmission (as discussed in section 2.3.1),

τ_c = cloud energy transmission (as discussed in section 2.3.2),

τ_{cw} = cloud to water energy transmission (as discussed in section 2.3.3),

τ_{aw} = air-water interface energy transmission (as discussed in sections 2.3.4 and 2.3.6),

τ_w = water energy transmission (as discussed in section 2.3.7), and

$I(\phi^w)$ = water radiance distribution (as discussed in section 2.3.8).

Therefore, the received optical energy is given by

$$E_R = \left(\frac{E_p \gamma_T}{(\pi \theta^2_T/4)} \right) \left(\frac{(\pi d^2/4)\, \gamma_R}{R^2} \right) \tau_a \tau_c \tau_{cw} \tau_{aw} \tau_w f(\phi_o, \theta_R) \ . \tag{S-36}$$

*This assumes such large spots that additional cloud and water spreading is negligible.

The fraction of the incident radiance within the receiver field-of-view is given by (for perfect alignment between beam axis and receiver axis):

$$f(\Omega) = \frac{\int_0^{2\pi} \int_0^{\theta_R} I(\phi^W)\, d\Omega}{\int_0^{2\pi} \int_0^{\phi_o} I(\phi^W)\, d\Omega} \quad , \quad \theta_R < \phi_o \quad ; \tag{S-37}$$

for

θ_R = half angle of the receiver field-of-view, and

ϕ_o = off-axis angle at which incoming radiance equals zero.

Using the model adopted in section 2.3.8,

$$f(\Omega) = f(\phi_0, \theta_R) = \frac{1 - \cos\theta_R - \frac{1}{3\sin^2\phi_0}\left[\cos\theta_R \sin^2\theta_R + 2\cos\theta_R - 2\right]}{1 - \cos\phi_0 - \frac{1}{3\sin^2\phi_0}\left[\cos\phi_0 \sin^2\phi_0 + 2\cos\phi_0 - 2\right]} \tag{S-38a}$$

and, $f(\phi_o, \theta_R) = 1$, for $\theta_R > \phi_o$. (S-38b)

Using equations (S-36), (S-27), and (S-33) results in the evaluation of the instantaneous optical power in terms of all the other signal group sub-models.

3.0 NOISE PROPAGATION GROUP

This section discusses the proposed equation group for the propagation of the noise relative to a single signal pulse.

3.1 OBJECTIVE, STRUCTURE, AND FUNCTION

This section considers the basic approach used in the detailed noise calculation modules presented in section 3.3, and presents flow charts showing the interrelationship of these sub-models and their required inputs. (These inputs are discussed in more detail in section 3.2.)

3.1.1 Philosophy of Approach

Since all the background sources that must propagate through clouds are continuous in time, that part of the modeling related to the temporal effects is not present here. This simplifies the noise modeling.

On the other hand, the sources of the noise are so different (sun, moon, sky-light, star-light, bioluminescence, shot noise in the receiver amplifier, detector dark current, etc.), that is has been difficult to develop a single unified approach to all of them. The approach, therefore, is described below.

Express the noise contribution as a noise-equivalent-optical-power (NEP_{tot}), which is the root sum of squares of all the noise-equivalent-optical power contributions of the individual noise components. The NEP_{tot} is then directly comparable to the instantaneous received optical power $P_R(t)$ developed in section 2, and the signal-to-noise ratio is P_R/NEP_{tot}; for P_R the peak value of the received signal power.

Take the out-of-water background sources in terms of equivalent exo-atmospheric radiances, and then their propagation through the atmosphere and water path is treated in parallel with the signal energy transmission of section 2.3. The angular effects and noise radiance distribution are also treated in a manner similar to that of the signal in section 2.

Take the noise contributions of the background sources as the 1-sigma point in the fluctuations generated in the signal current by their steady presence, and express their contributions in terms of an equivalent optical power.

Treat the amplifier shot noise, detector dark current and signal shot noise in the standard way, and express their contributions in terms of an equivalent optical power.

Present the modeling in modular fashion, so that the effect of each portion of the path is evident. In addition, as further experiments and analysis are undertaken, pieces of the model may be upgraded without requiring extensive modifications to this publication or the total model.

Separate the cloud conditions into clear/thin cloud, corresponding to an optical thickness (τ_{opt}) < 10 and thick cloud for $\tau_{opt} > 10$. Below $\tau_{opt} = 10$ one set of noise-modules is assumed to apply, while above it a different set applies. In many cases these noise modules do not correspond at $\tau_{opt} = 10$, and so the overall model should only be used for $\tau_{opt} < 10$ and $\tau_{opt} > 10$. (Further analysis and experiments on the "multiple forward scattering" region should enable these sub-models to be upgraded, and this inconsistency removed.)

Finally, we assume appropriate and simple analytic forms for at-present unknown functions such as the radiance distributions. This enables us to generate analytic results (except for the receiver axis offset from the beam axis of the incident radiation), which is an aid to a physical understanding of the situation.

3.1.2 Noise Group Structure

A schematic of the overall noise equivalent power propagation group is shown in figure 19. Given the input parameters, the path energy transmission and angular and radiance distributions are derived for the four "exo-atmospheric" background sources. Then, using additional input data, the average background power for all background sources is derived, and so, the noise-equivalent optical power for all the noise components.

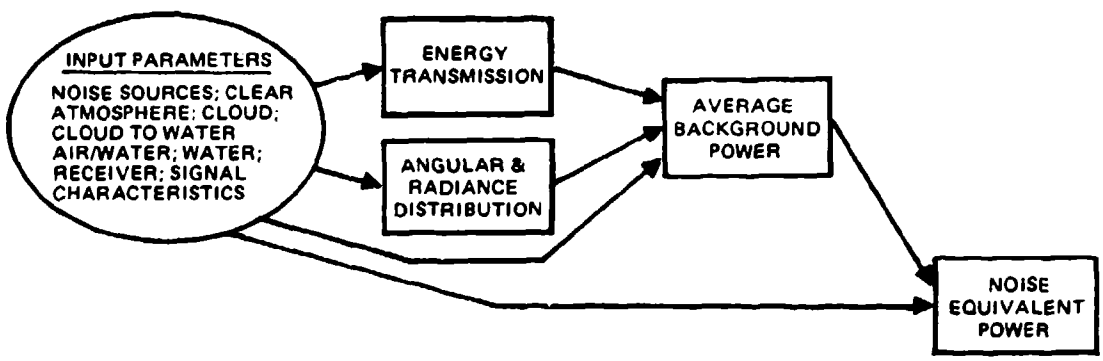

Figure 19. Schematic of single-pulse noise equivalent power downlink propagation group.

Figure 20 is a detailed flow diagram of the direct sunlight contribution, showing the calculations that must be performed to arrive at the required output. (The flow charts for the moonlight, blue sky-light and starlight/zodiacal light are identical to this one, while the simpler one for the bioluminscence is shown in figure 21.) The following six steps are used to exercise the noise propagation group:

- The input parameters are listed in the eight ellipses on the left-hand side of the figure including source, clear atmosphere, cloud, cloud to water, air-water interface, water, receiver and signal characteristic parameters. (The symbols are defined in the glossary and also in the input discussion in section 3.2.)
- The primary calculation equations are represented by the rectangular boxes. Within each box is the symbol for the parameter to be calculated and the equation number (from section 3.3) for the equation to be used to calculate that parameter.
- The first quantity calculated is the cloud optical thickness, τ_{opt}, since this determines which equations should be used to calculate many other parameters. Whenever // appears in a rectangular box, the equation number preceeding it refers to $\tau_{opt} > 10$, while the equation number following it refers to $\tau_{opt} < 10$. Hence, given the value of τ_{opt}, the rest of the models to be used are specifically determined.

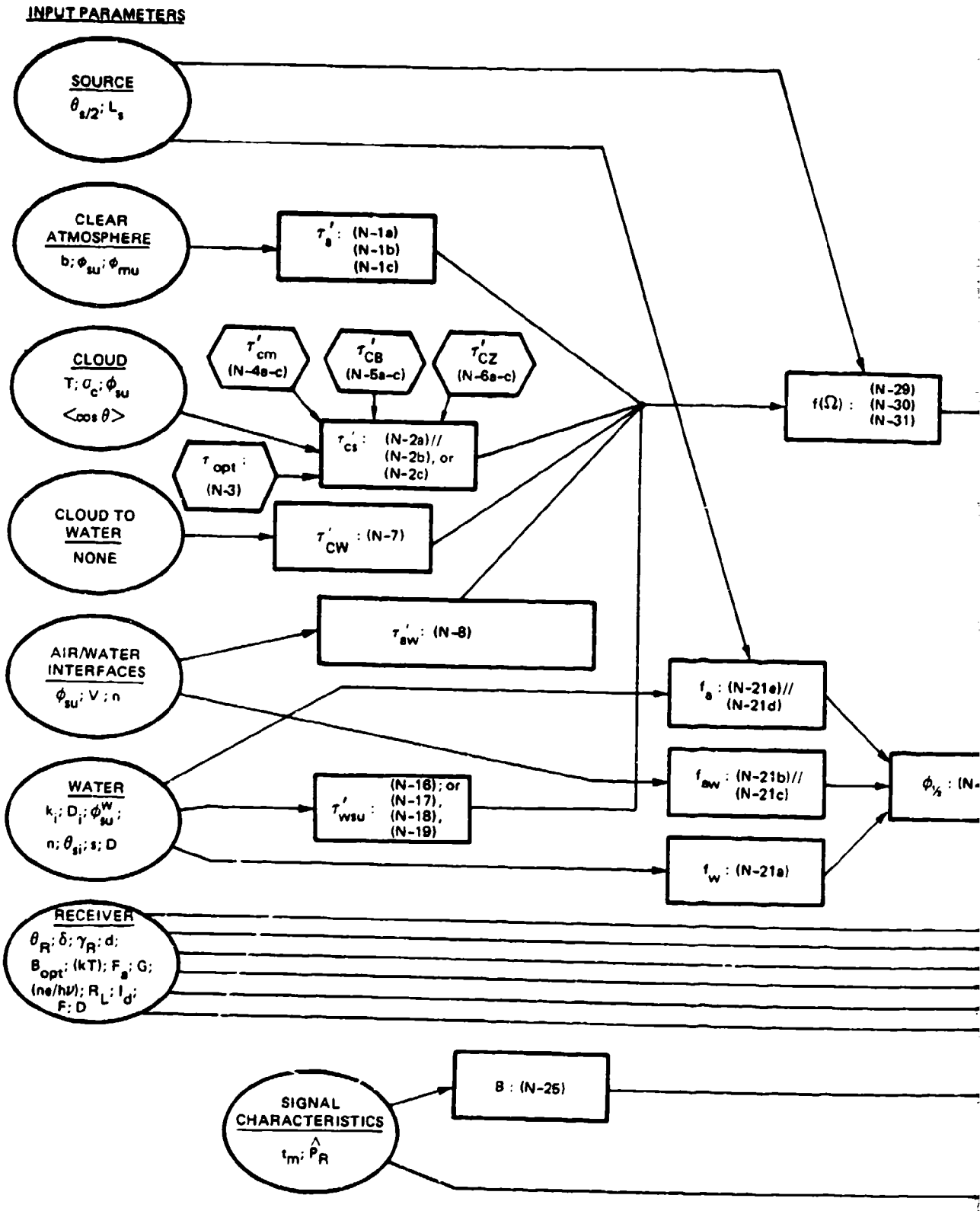
INPUT PARAMETERS
SOURCE
$\theta_{s/2}$; L_s
CLEAR ATMOSPHERE
b; ϕ_{su}; ϕ_{mu}
τ'_a: (N-1a) (N-1b) (N-1c)
CLOUD
T; σ_c; ϕ_{su}
$\langle \cos\theta \rangle$
τ'_{cm} (N-4a-c)
τ'_{CB} (N-5a-c)
τ'_{CZ} (N-6a-c)
τ'_{cs}: (N-2a)// (N-2b), or (N-2c)
τ_{opt}: (N-3)
CLOUD TO WATER
NONE
τ'_{CW}: (N-7)
τ'_{aw}: (N-8)
AIR/WATER INTERFACES
ϕ_{su}; V; n
WATER
k_i; D_i; ϕ^w_{su}; n; θ_{si}; s; D
τ'_{wsu}: (N-16); or (N-17), (N-18), (N-19)
RECEIVER
θ_R; δ; γ_R; d; B_{opt}; (kT); F_a; G; (ne/hν); R_L; I_d; F; D
SIGNAL CHARACTERISTICS
t_m; $\hat{P}_R$
B: (N-25)
$f(\Omega)$: (N-29) (N-30) (N-31)
f_a: (N-21e)// (N-21d)
f_{aw}: (N-21b)// (N-21c)
f_w: (N-21a)
$\phi_{½}$: (N-

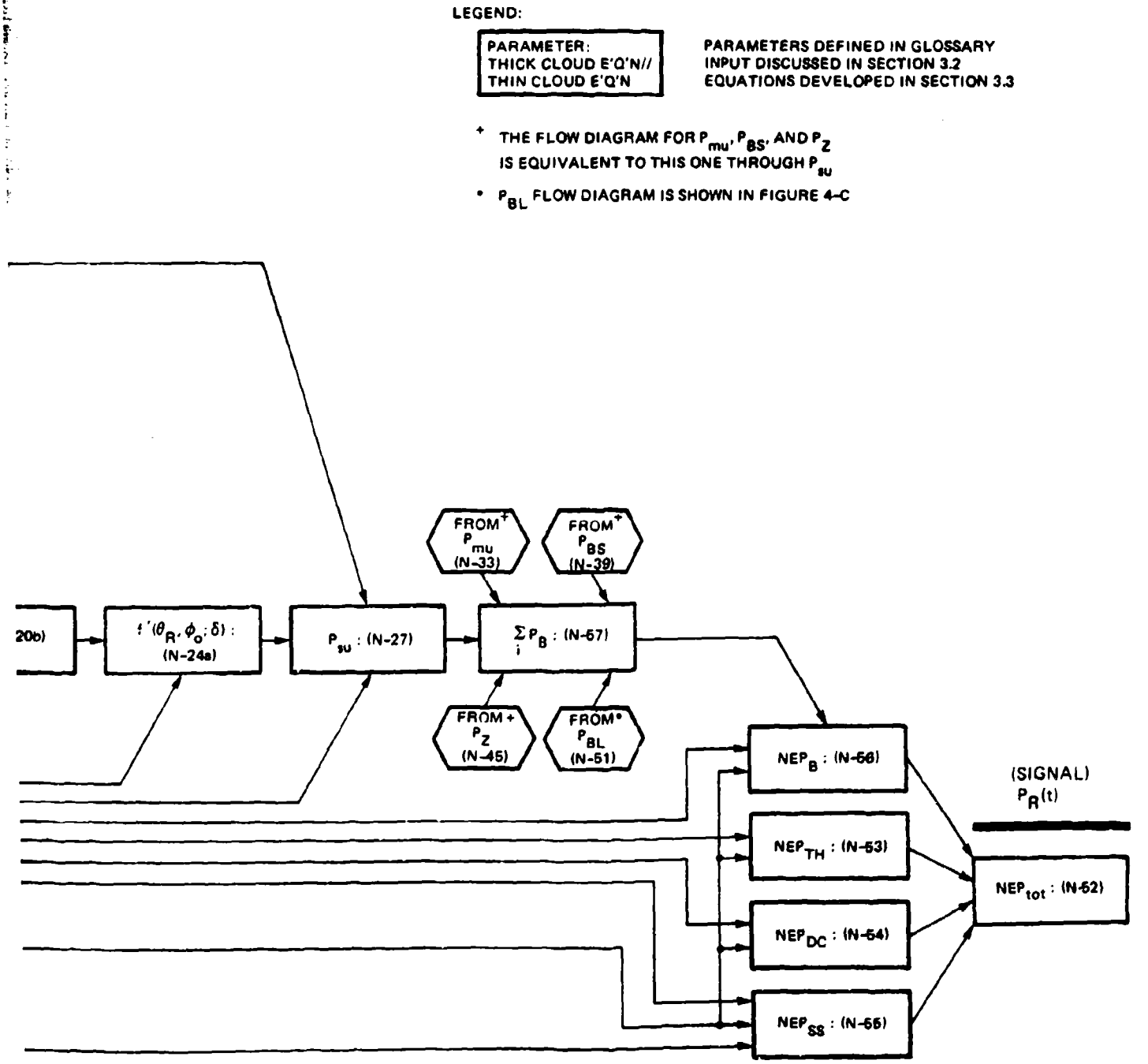

Figure 20. Flow diagram of single-pulse downlink noise propagation group.

- The second set of calculations performed are of two types:
  (a) path transmission, including τ'_a, τ'_c, τ'_{cw}, τ'_{aw}, and τ'_w; and,
  (b) angular and radiance distribution including f_a, f_{aw}, f_w, ϕ_o and $f'(\theta_R \phi_o, \delta)$.
- The path transmission, angular and radiance distribution, source and receiver parameters are then used to calculate the average background power due to that source.
- The total average background power due to all sources is then calculated.
- The total average background power, receiver and signal characteristics are then used to calculate the total noise equivalent optical power.

Figure 21 shows the flow chart for calculating the average background power due to bioluminescence, P_{BL}. This value of P_{BL} enters into figure 20 in the $\Sigma_1^i P_B$ calculations.

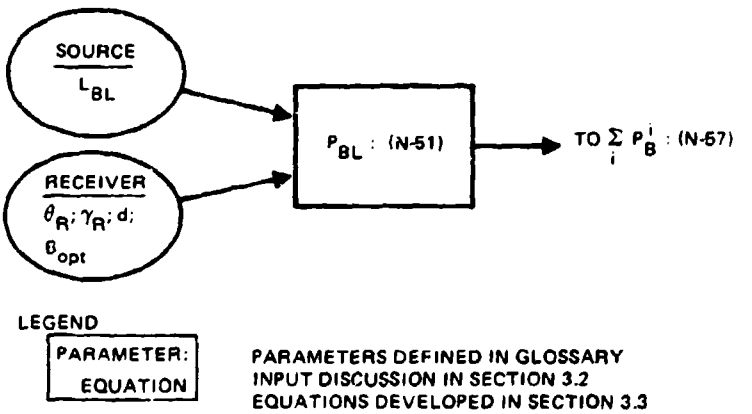

Figure 21. Flow diagram of single-pulse downlink noise propagation submodel (noise due to bioluminescence).

3.2 INPUT FOR NOISE CALCULATION

This section discusses the form (and values in some cases) of the required inputs to the noise group, in terms of the eight categories: source, clear atmosphere, cloud, cloud to water, air-water interface, water, receiver and signal characteristics.

3.2.1. Source

There are five sources of the average background, which are treated here as independent. These sources are: sunlight, moonlight, blue skylight, starlight/zodiacal light, and bioluminescence.

It is expected that these sources will be treated rationally when using them as inputs, so that when sunlight is present, only the blue-skylight will be expected to be a non-zero value; and when moonlight is present only the starlight/zodiacal light and bioluminescence will be used with non-zero values. (A full diurnal model for these sources is not considered appropriate at this time.)

We consider each of the five noise sources separately.

SUN

Symbol	Description	Units
$\theta_{s/2}$	The half-angle subtended by the sun at the earth. Its value is taken as (ref 10): $4.65\ 10^{-3}$ radians.	radians
$H_{s\lambda}$	Effective exo-atmospheric spectral radiance of the sun. The value assumed will be 2000 watts/m^2 - μ.	watts/(metres)^2 (microns)

MOON

Symbol	Description	Units
$\theta_{m/2}$	The half-angle subtended by the moon at the earth. Its value is equal to (ref 11): $\theta_{s/2} = 4.65\ (10^{-3})$ radians.	radians
$H_{mu\lambda}$	Effective exo-atmospheric spectral irradiance of the moon. It will be assumed to equal 4.3 watts/m^2 - μ.	$\frac{\text{watts}}{(\text{metres})^2(\text{microns})}$

STARLIGHT/ZODIACAL LIGHT

Symbol	Description	Units
L_Z	Effective exo-atmospheric spectral radiance due to all non-lunar night time sources. The value (ref 12) is $3\ (10^{-6})$ [watts/(metres)^2(srad)(micron)] in the blue-green spectral region.	[watts/(metres)^2 (steradians) (microns)]

BIOLUMINESCENCE

Symbol	Description	Units
L_{BL}	Spectral irradiance of the ambient bioluminescence sources at the aperture of the submarine receiver. The value for this parameter is least well known of all the background contributors. As previously done, and until further information is available, we use the values provided in the SAOCS RFP, so that (ref 13) $L_{BL} = (10^{-3})$ watts/m^2 microns.	[watts/(metres)^2 (microns)]

BLUE SKYLIGHT

Symbol	Description	Units
L_B	Effective exo-atmospheric spectral radiance of the blue-sky. Its value is assumed to be 250 watts/[(metres)^2(srad)(micron)]	[watts/(metres)^2 (microns)]

10. Handbook of Geophysics (rev ed), p 17-1, 17-2, MacMillan Co, New York, 1960.
11. RC Haynes, Introduction to Space Service, p 4-5, John Wiley and Sons, New York, 1971.
12. WK Pratt, Laser Communication Systems, ref 4, p 122, fig 6-7, John Wiley and Sons, New York, 1969.
13. NOSC Interim Report No. 2, Contract No N00039-77-C-0100, Optical Submarine Communication by Aerospace Relay (OSCAR) (U), T Flom, PF Titterton, et al., p 3-22 to 3-24, Secret, 1 May 1978.

3.2.2 Clear Atmosphere

The required parameters are:

Symbol	Description	Units
b	Effective clear atmospheric optical thickness. For a zenith transmission of 70%; b = 0.357	
ϕ_{su}	In-air solar zenith angle	radians
ϕ_{mu}	In-air lunar zenith angle	radians

3.2.3 Cloud

The required parameters are:

Symbol	Description	Units
T	Geometric or physical thickness of the cloud.	metres
σ_c	Average extinction coefficient of the cloud.	$(\text{metres})^{-1}$
ϕ_{su}	In-air solar zenith angle	radians
ϕ_{mu}	In-air lunar zenith angle	radians
$\langle\cos\theta\rangle$	The average value of the cosine of the scattering angle for single scattering within the cloud.	

3.2.4 Cloud to Water

No parameters in this area affect the noise properties.

3.2.5 Water

The required parameters are:

Symbol	Description	Units
k_i	Diffuse attenuation coefficient of the i'th water layer.	$(\text{metres})^{-1}$
D_i	Thickness of the i'th water layer	(metres)
ϕ_{su}^{w}	In-water solar zenith angle	radians
ϕ_{mu}^{w}	In-water lunar zenith angle	radians
n	Water index of refraction	
θ_{si}	Root-Mean-Square angle for a single scattering event in the water.	radians
s	Scattering coefficient for the entire water path	$(\text{metres})^{-1}$
D	Depth of the submarine receiver	metres

3.2.6 Air/Water Interface

The required parameters are:

Symbol	Description	Units
ϕ_{su}	In-air solar zenith angle	radians
ϕ_{mu}	In-air lunar zenith angle	radians
v	Surface wind speed	metres/second
n	Water index of refraction	

3.2.7 Receiver

The required parameters are:

Symbol	Description	Units
θ_R	Half-angle of the receiver field of view	radians
δ	Off-set angle between the in-water noise source beam and the receiver optical axis	radians
γ_R	Transmission of the receiver optical aperture	
d	Diameter of the receiver optical aperture	metres
B_{opt}	Passband of the optical filter	microns
(kT)	Thermal noise contribution in the amplifier	Joules
F_a	Excess amplifier noise o' ' thermal noise	
G	Gain of the photo-detector	
$(\eta e/h\nu)$	Responsivity of the photo-surface	amps/Watts
R_L	Load resistance following the photo-detector	Ohms
I_d	Dark current at the detector cathode	amps
F	Excess noise in the photo-detector gain	
D	Depth of the submarine receiver	metres

3.2.8 Signal Characteristics

Two parameters from the signal characteristics which enter into the Noise calculations are:

Symbol	Description	Unit
t_m	Time after pulse initiation at which it peaks, for a t exp - (t/t_m) shape.	seconds
$\hat{P}_R$	Peak value of the received optical signal power.	watts

3.3 NOISE CALCULATION MODULES

This section develops all the equations used in the calculation of the noise contribution to the total noise equivalent optical power.

Sections 3.3.1, 3.3.2, 3.3.3, 3.3.4, 3.3.6, and 3.3.7 consider the path transmission of the energy.

Sections 3.3.5 and 3.3.8 consider the angular effects and the distribution of the received radiance.

Section 3.3.9 considers the electrical detection bandwidth in terms of the received pulse width.

In each of these sections, after the equations are developed they are evaluated for typical cases in both tables and figures.

Sections 3.3.10 and 3.3.14 then derive the average background optical power for the five types of background sources, and Section 3.3.15 presents the expression for the total noise equivalent optical power due to all noise sources.

3.3.1 Clear Atmospheric Transmission

In the absence of any clouds or aerosols, the clear atmospheric transmission is described by the term τ'_a. Using the approximate AFCRL model (ref 1), the solar (or lunar) zenith angle dependence is given by:

$$\boxed{\tau'_a = \exp(-b \sec \phi_{su})} \quad , \qquad \text{(N-1a)} \qquad \boxed{\tau'_a = \exp(-b \sec \phi_{mu})} \qquad \text{(N-1b)}$$

for

τ'_a = solar (or lunar) clear atmospheric transmission

b = effective clear atmosphere optical thickness

ϕ_{su} = solar zenith angle. While conversely,

ϕ_{su} is replaced by ϕ_{mu} = lunar zenith angle.

The typical value of b is determined by

$$\tau'_a(\phi_{su} = 0) = 0.7 = \exp(-b) \quad ,$$

or

$$b = 0.357.$$

Table 12 and figure 22 show the values of τ'_a as a function of solar zenith angle.

The other two out-of-water sources of background radiation are taken as uniformly distributed over the hemisphere. Then the effective atmospheric transmission is weighted by the transmission at each zenith angle, or, for the blue-sky and the stellar sources,

$$\tau'_a = \frac{\int_0^{2\pi} d\phi \int_0^{\pi/2} \sin\theta \, d\theta \exp - [b \sec \theta]}{\int_0^{2\pi} d\phi \int_0^{\pi/2} \sin\theta \, d\theta}$$

Table 12. Typical clear atmospheric transmission (b = 0.357).

ϕ'_{su}, Solar Zenith Angle	τ'_a, Clear Atmospheric Transmission
0	0.7
10	0.7
20	0.68
30	0.66
40	0.63
50	0.57
60	0.49
70	0.35
80	0.13

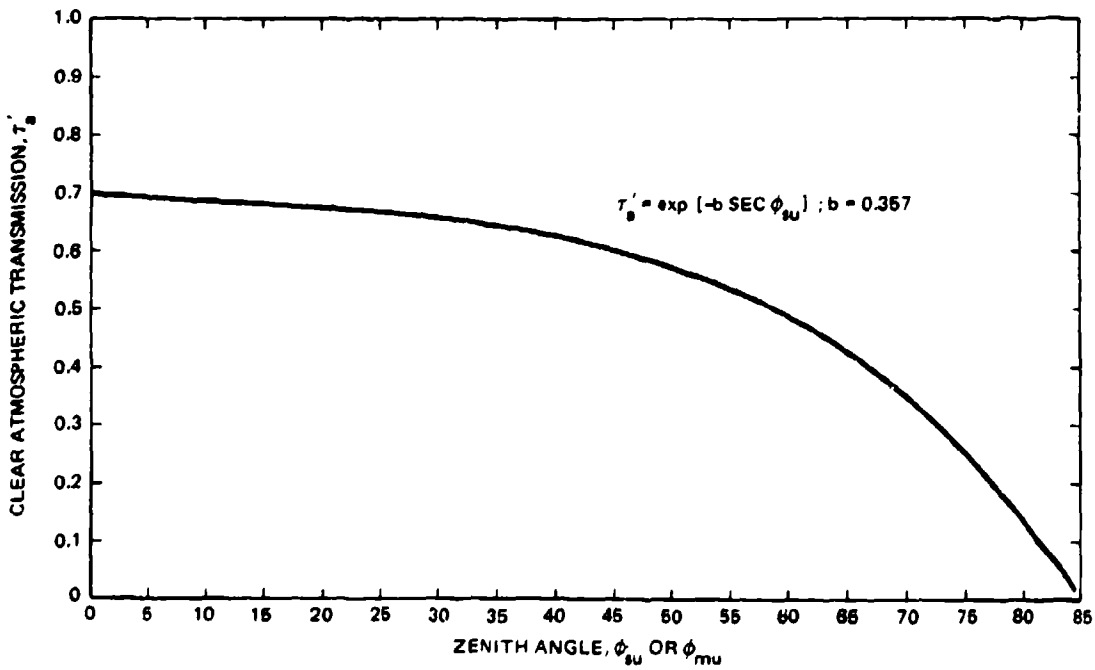

Figure 22. Typical clear atmospheric transmission (b = 0.357).

$$\tau'_a = E_2(b) \quad \text{for blue sky or stellar background} \quad , \tag{N-1c}$$

with $E_2(b)$ = exponential integral (ref 14). For b = 0.357, E_2 (0.357) = 0.42.

14. Handbook of Mathematical Functions, M Abramowitz and IA Stegun, eds, p 228, NBS Applied Mathematics Series 35, GPO. November 1970.

3.3.2 Cloud Energy Transmission

The transmission of sunlight or moonlight by clouds does not have an experimentally verified expression. Most work in cloud transmission has been a broadband treatment of transmitted irradiance (watts/m^2), and there have been no experiments which collected the total energy emerging from thick or thin clouds.

We propose to adopt a number of different (but consistent) models, depending on the characteristics of the noise source.

For the sun and moon we shall adopt the same model as for the signal (section 2.3.2), with the exception that both the sunlight and moonlight do spread out with zenith angle, and thus the extra cosine factor is always present.

Therefore, for the sun,

$$\tau'_{cs} = \left\{ \frac{A(\phi_{su})}{\tau_{opt}(1 - \langle\cos\theta\rangle) + 1.42} \right\} \left\{ 2\sqrt{3(1 - \langle\cos\theta\rangle)(1 - \omega_0)} \right\} \left\{ \tau_{opt} + \frac{1.42}{1 - \langle\cos\theta\rangle} \right\}$$

$$\times \left\{ \frac{\exp - \left[\sqrt{3(1 - \langle\cos\theta\rangle)(1 - \omega_0)} \left\{ \tau_{opt} + \frac{1.42}{1 - \langle\cos\theta\rangle} \right\} \right]}{1 - \exp - \left[2\sqrt{3(1 - \langle\cos\theta\rangle)(1 - \omega_0)} \left\{ \tau_{opt} + \frac{1.42}{1 - \langle\cos\theta\rangle} \right\} \right]} \right\}$$

$$\times \left| \cos\phi_{su} \right|^{1.0} ; \qquad \text{for } \tau_{opt} \geq 10. \tag{N-2a}$$

$$\tau'_{cs} = \left\{ 1 - 0.085\,\tau_{opt} \left[\frac{1.69}{10(1 - \langle\cos\theta\rangle) + 1.42} \right] \right\} \left| \cos\phi_{su} \right|^{2} ; \qquad \text{for } \tau_{opt} \leq 10. \tag{N-2b}$$

$$\tau'_{cs} = \cos\phi_{su}; \qquad \text{for } \tau_{opt} = 0 . \tag{N-2c}$$

where

τ'_{cs} = cloud energy transmission of direct sunlight,

τ_{opt} = optical thickness of the cloud

$\langle\cos\theta\rangle$ = mean cosine of the scattering angle,

and ϕ_{su} = solar zenith angle. $A(\phi_s)$ was given in equation (S-4) of section 2.3.2.
As before,

$$\tau_{opt} = T\,\sigma_c \ , \tag{N-3}$$

Here,

T = geometrical thickness of the cloud, and

σ_c = mean extinction coefficient of the cloud.

For the moon,

$$\tau'_{cm} = \left| \frac{A(\phi_{mu})}{\tau_{opt}(1 - \langle\cos\theta\rangle) + 1.42} \right| \left| 2\sqrt{3(1 - \langle\cos\theta\rangle)(1 - \omega_0)} \right| \left| \tau_{opt} + \frac{1.42}{1 - \langle\cos\theta\rangle} \right|$$

$$\times \left\{ \frac{\exp - \left[\sqrt{3(1 - \langle\cos\theta\rangle)(1 - \omega_0)} \left| \tau_{opt} + \frac{1.42}{1 - \langle\cos\theta\rangle} \right| \right]}{1 - \exp - \left[2\sqrt{3(1 - \langle\cos\theta\rangle)(1 - \omega_0)} \left| \tau_{opt} + \frac{1.42}{1 - \langle\cos\theta\rangle} \right| \right]} \right\}$$

$$\left| \cos\phi_{mu} \right|^{1.0} \quad ; \qquad \text{for } \tau_{opt} \geq 10. \tag{N-4a}$$

and

$$\tau'_{cm} = \left\{ 1 - 0.085\, \tau_{opt} \left[\frac{1.69}{10(1 - \langle\cos\theta\rangle) + 1.42} \right] \right\} (\cos\phi_{mu})^2 \quad ; \qquad \text{for } \tau_{opt} \leq 10. \tag{N-4b}$$

Also,

$$\tau_{cm} = \cos\phi_{mu} \qquad \text{for } \tau_{opt} = 0. \tag{N-4c}$$

Here,

τ'_{cm} = cloud energy transmission of direct moonlight,

and

ϕ_{mu} = lunar zenith angle.

The typical energy transmission (for $\langle\cos\theta\rangle = 0.83$) described by equations (N-2) and (N-4) is shown in table 13 and figure 23.

The zenith angle dependence for both regimes of τ_{opt} is shown in table 14 and figure 24.

Again, there is a discontinuity in the zenith angle dependence at $\tau_{opt} = 10$, which we shall ignore pending a verified model of cloud energy transmission

The other two out-of-water sources of the ambient background are approximated as uniform sources distributed across the full hemisphere. Then, an extra factor arises due to their distribution in angle of incidence upon the cloud. This extra factor is given by

$$\int_0^{\pi/2} f(\phi) \sin\phi \, d\phi \quad ;$$

for $f(\phi)$ = $A(\phi)$ for thick clouds,

= $\cos\phi$ for thin clouds, and

ϕ = zenith angle of the incident light.

Table 13. Typical energy transmission for sunlight and moonlight at zenith ($\langle \cos\theta \rangle = 0.83$, $\omega_0 = 1$.

τ_{opt}, Optical Thickness	τ'_{cs}, τ'_{cm}, Cloud Energy Transmission
0	1
2	0.91
4	0.82
6	0.72
8	0.63
10	0.54
20	0.35
30	0.26
40	0.21
50	0.17
60	0.15
70	0.13
80	0.11
90	0.10
100	0.09

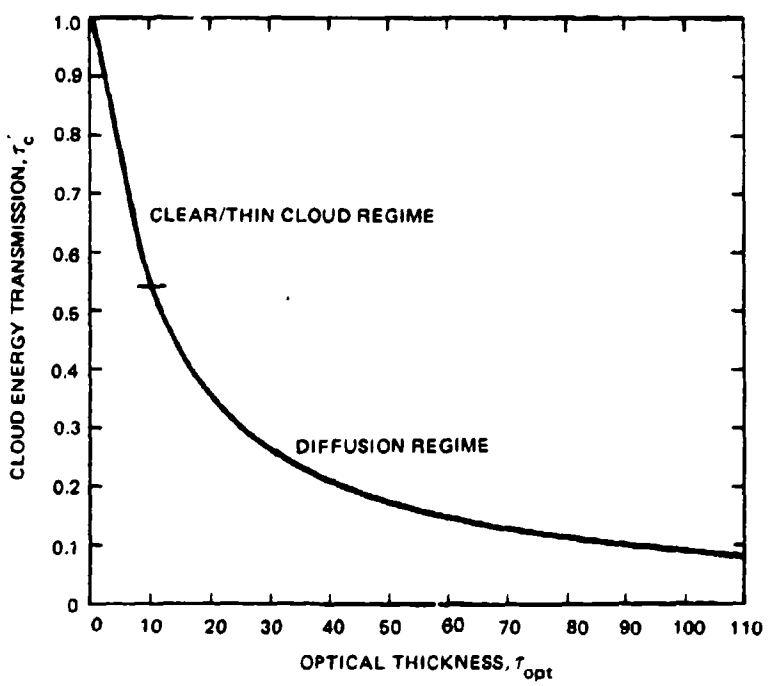

Figure 23. Thick and thin cloud energy transmission versus optical thickness, for $\langle \cos\theta \rangle = 0.83$. $\omega_0 = 1$.

Table 14. Zenith angle dependence of sun and moon cloud energy transmission (normalized to $\phi_{su} = 0$ and $\phi_{mu} = 0$).

ϕ_{su}, ϕ_{mu} Zenith Angle	Thick Cloud Dependence ($\tau_{opt} \geq 10$)	Thin Cloud Dependence ($\tau_{opt} < 10$)
0	1	1
10	0.96	0.97
20	0.90	0.88
30	0.79	0.75
40	0.66	0.59
50	0.50	0.41
60	0.34	0.25
70	0.20	0.12
80	0.08	0.03
85	0.03	0.008

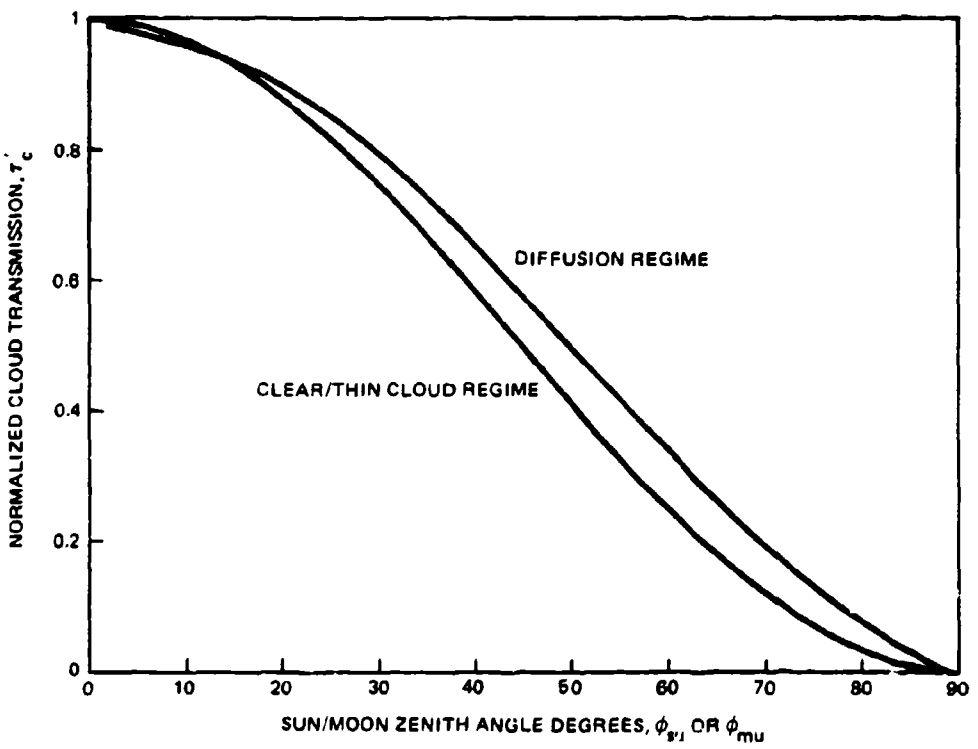

Figure 24. Thin and thick cloud zenith angle dependence of cloud transmission normalized to zenith.

Evaluating this integral we find it equals 0.6695 (expressed 2/3) for thick clouds and 0.5 (expressed 1/2) for thin ones. Therefore, for the blue sky background, the cloud energy transmission is given by:

$$\tau'_{CB} \approx \frac{2}{3}\left\{\frac{1.69}{\tau_{opt}(1-\langle\cos\theta\rangle)+1.42}\right\}\left\{2\sqrt{3(1-\langle\cos\theta\rangle)(1-\omega_0)}\right\}\left\{\tau_{opt}+\frac{1.42}{1-\langle\cos\theta\rangle}\right\} \times\left\{\frac{\exp-\left[\sqrt{3(1-\langle\cos\theta\rangle)(1-\omega_0)}\left\{\tau_{opt}+\frac{1.42}{1-\langle\cos\theta\rangle}\right\}\right]}{1-\exp-\left[2\sqrt{3(1-\langle\cos\theta\rangle)(1-\omega_0)}\left\{\tau_{opt}+\frac{1.42}{1-\langle\cos\theta\rangle}\right\}\right]}\right\}; \quad \text{for } \tau_{opt} \geq 10. \tag{N-5a}$$

$$\tau'_{CB} = \frac{1}{2}\left\{1-0.085\,\tau_{opt}\left[\frac{1.69}{10(1-\langle\cos\theta\rangle)+1.42}\right]\right\}; \quad \text{for } \tau_{opt} < 10. \tag{N-5b}$$

$$\tau'_{CB} = 1, \text{ for } \tau_{opt} = 0\ . \tag{N-5c}$$

The discontinuity at $\tau_{opt} = 10$ is again present, and again neglected until a better experimental model is derived.

Note equation (N-5a, b) are independent of solar zenith angle. However, the strength of the radiance incident from the blue sky does depend on solar zenith angle.

For the moonless night case, the stellar/zodiacal light cloud energy transmission is given by

$$\tau'_{CZ} \approx \frac{2}{3}\left\{\frac{1.69}{\tau_{opt}(1-\langle\cos\theta\rangle)+1.42}\right\}\left\{2\sqrt{3(1-\langle\cos\theta\rangle)(1-\omega_0)}\right\}\left\{\tau_{opt}+\frac{1.42}{1-\langle\cos\theta\rangle}\right\} \times\left\{\frac{\exp-\left[\sqrt{3(1-\langle\cos\theta\rangle)(1-\omega_0)}\left\{\tau_{opt}+\frac{1.42}{1-\langle\cos\theta\rangle}\right\}\right]}{1-\exp-\left[2\sqrt{3(1-\langle\cos\theta\rangle)(1-\omega_0)}\left\{\tau_{opt}+\frac{1.42}{1-\langle\cos\theta\rangle}\right\}\right]}\right\}; \quad \text{for } \tau_{opt} \geq 10, \tag{N-6a}$$

$$\tau'_{CZ} = \frac{1}{2}\left\{1 - 0.085\,\tau_{opt}\left[\frac{1.69}{10\,(1 - \langle\cos\theta\rangle) + 1.42}\right]\right\}; \quad \text{for } \tau_{opt} < 10, \tag{N-6b}$$

$$\tau'_{CZ} = 1, \text{ for } \tau_{opt} = 0 \quad . \tag{N-6c}$$

Table 15 and figure 25 show a typical cloud energy transmission as a function of cloud optical thickness for these uniform sources of ambient background.

Table 15. Typical cloud energy transmission for blue skylight and stellar/zodiacal light ($\langle\cos\theta\rangle = 0.83$, $\omega_0 = 1$).

τ_{opt}, Optical Thickness	τ'_{cb}, τ'_{cz} Cloud Energy Transmission
0	1
2	0.46
4	0.41
6	0.36
8	0.32
10	0.27 (thin); 0.36 (thick)
20	0.23
30	0.17
40	0.14
50	0.11
60	0.1
70	0.087
80	0.073
90	0.067
100	0.06

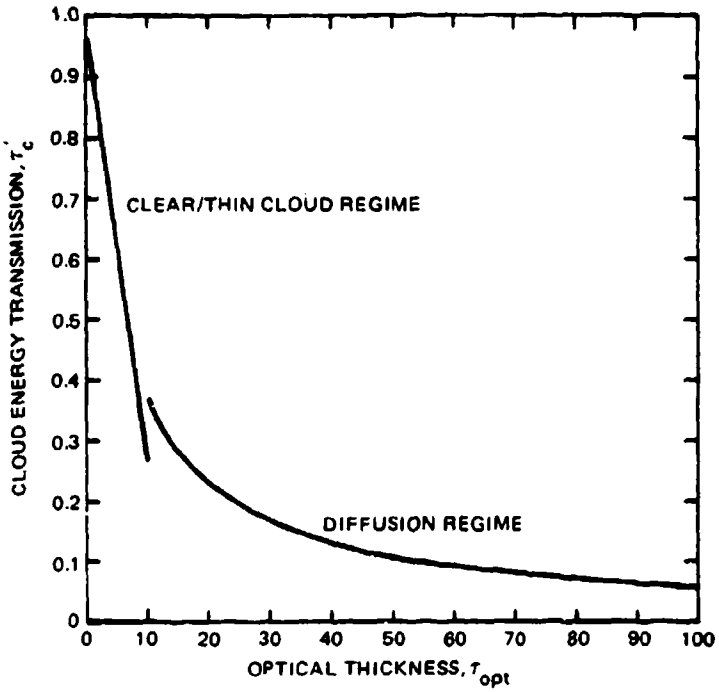

Figure 25. Typical cloud energy transmission for blue skylight and stellar light ($<\cos\theta> = 0.83$, $\omega_0 = 1$).

3.3.3 Cloud to Water Energy Transmission

Because the sun and moon are effectively sources of infinite plane waves, and the blue sky and stellar background cover the entire hemisphere, there is no "spot" or "beam" enlargement in propagation from the cloud base to the water surface. Therefore, the transmission of noise energy from cloud base to the water surface is given by:

$$\boxed{\tau'_{cw} = 1,} \qquad \text{(N-7)}$$

for all cloud conditions.

3.3.4 Air-Water Transmission

The energy transmission of the air-water interface is composed of two factors:

$$\boxed{\tau'_{aw} = (\tau'_{aw1}) \times (\tau'_{aw2}) \ ;} \qquad \text{(N-8)}$$

for,

τ'_{aw} = total energy transmission of air-water interface,

τ'_{aw1} = air-water interface transmission due to index of refraction discontinuity, and

τ'_{aw2} = air-water interface transmission due to foam and streaks on the sea surface.

This section treats τ'_{aw1}, while τ'_{aw2} is discussed in section 3.3.6. For thin clouds and clear weather ($\tau_{opt} \leq 10$) the solar and lunar energy transmission is again given as a function of wind speed and solar/lunar zenith angle in table 16 and figure 26.

Table 16. $\tau'_{awls}/\tau'_{awlm}$ time averaged downlink air-sea interface transmittance (for thin clouds, $\tau_{opt} \leq 10$).

ϕ_s Signal Zenith Angle in Air	V_l Wind Speed								
	0	1.03	2.06	4.12	7.21	10.3	13.4	16.5	19.6 m/sec
	0	2	4	8	14	20	26	32	38 knots
0	0.979	0.977	0.976	0.974	0.970	0.967	0.963	0.960	0.956
5	0.975	0.974	0.972	0.970	0.966	0.963	0.959	0.956	0.952
10	0.964	0.962	0.961	0.959	0.955	0.951	0.948	0.944	0.941
15	0.945	0.944	0.943	0.940	0.936	0.933	0.929	0.926	0.922
20	0.920	0.918	0.917	0.914	0.910	0.907	0.903	0.899	0.896
25	0.887	0.885	0.884	0.881	0.877	0.873	0.870	0.866	0.863
30	0.847	0.845	0.844	0.841	0.837	0.833	0.829	0.826	0.822
35	0.800	0.798	0.797	0.794	0.790	0.786	0.782	0.779	0.775
40	0.747	0.745	0.743	0.741	0.736	0.733	0.729	0.725	0.722
45	0.687	0.685	0.684	0.681	0.677	0.673	0.669	0.666	0.663
50	0.620	0.619	0.617	0.615	0.611	0.608	0.605	0.602	0.599
55	0.548	0.546	0.545	0.543	0.540	0.538	0.536	0.534	0.532
60	0.469	0.468	0.468	0.466	0.465	0.464	0.464	0.464	0.463
65	0.385	0.385	0.385	0.386	0.387	0.389	0.391	0.393	0.395
70	0.295	0.298	0.299	0.303	0.310	0.315	0.321	0.325	0.329
75	0.203	0.209	0.214	0.224	0.236	0.247	0.255	0.262	0.268
80	0.113	0.126	0.136	0.153	0.172	0.186	0.197	0.206	0.213
85	0.0361	0.0610	0.0751	0.0969	0.119	0.135	0.148	0.157	0.165
90	0	0.0265	0.0390	0.0594	0.0809	0.0961	0.108	0.177	0.124

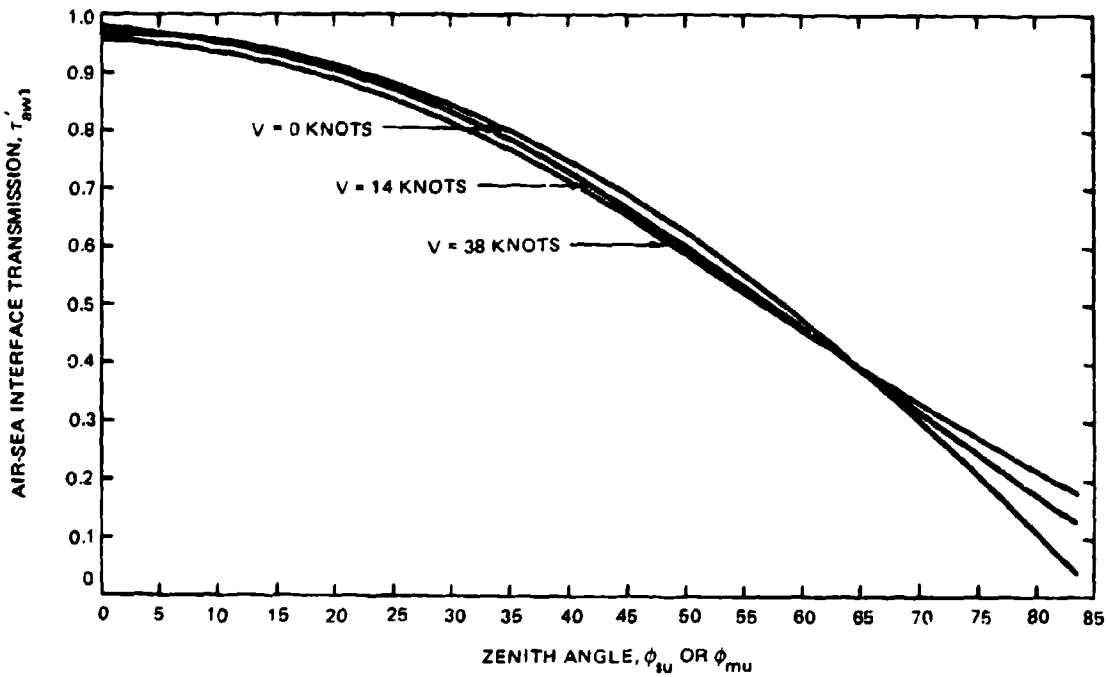

Figure 26. Air-sea interface transmittance as a function of sun or moon zenith angle and surface wind speed, v.

For diffuse or uniform radiation incident on the sea surface, we use the approximation in section 2.3.4 (which neglects wave effects) and take $\tau'_{aw1} = 0.83$.

$$\tau'_{aw1s} = 0.83, \quad \tau_{opt} \geq 10; \tag{N-9}$$

$$\tau'_{aw1m} = 0.83, \quad \tau_{opt} \geq 10; \tag{N-10}$$

and for blue sky,

$$\tau'_{aw1B} = 0.83, \quad \text{all values of } \tau_{opt}, \tag{N-11}$$

while for stellar/zodiacal light,

$$\tau'_{aw1Z} = 0.83, \quad \text{all values of } \tau_{opt}. \tag{N-12}$$

3.3.5 Air-Water Interface Angular Effects

The wave slopes on the sea surface cause an overall increase in the beam divergence of an incident beam, or equivalently, the apparent angular size of the source as viewed from an underwater point of view. With regard to the background sources, only the sun and moon for clear weather conditions ($\tau_{opt} \leq 10$) will be appreciably affected.

Again, using the Karp model discussed in section 2.3.5,

$$\Delta\theta_{aw}^{su,mu} = 0.0103\, v^{1/2} \quad (\tau_{opt} \leq 10)\,; \tag{N-13a}$$

for

$\Delta\theta_{aw}^{su}$ = rms induced half-angle spread for the sun, and

$\Delta\theta_{aw}^{mu}$ = rms induced half-angle spread for the moon.

v = surface wind speed in knots.

For all τ_{opt},

$$\Delta\theta_{aw}^{B,Z} = 0\,; \tag{N-14}$$

for

$\Delta\theta_{aw}D$ = effect on blue sky source, and

$\Delta\theta_{aw}Z$ = effect on stellar/zodiacal source.

Also

$$\Delta\theta_{aw}^{su,\,mu} = o, \quad (\tau_{opt} \geq 10), \tag{N-13b}$$

since the light is diffuse after emerging from the thick clouds.

Table 17 and figure 27 evaluate equation (N-13a) for V in knots (and metres per second).

Table 17. Rms air-water interface induced half-angle effects ($\tau_{opt} \leq 10$) sun and moon.

v, Wind Speed		$\Delta\theta_{aw}$ su or mu	
Knots	Metres/Sec	Milliradians	Degrees
0	0	0	0
2	1.03	14.6	0.84
4	2.06	20.7	1.18
8	4.12	29.2	1.67
14	7.21	38.6	2.21
20	10.3	46.2	2.65
26	13.4	52.6	3.0
32	16.5	58.4	3.35
38	19.6	63.6	3.64

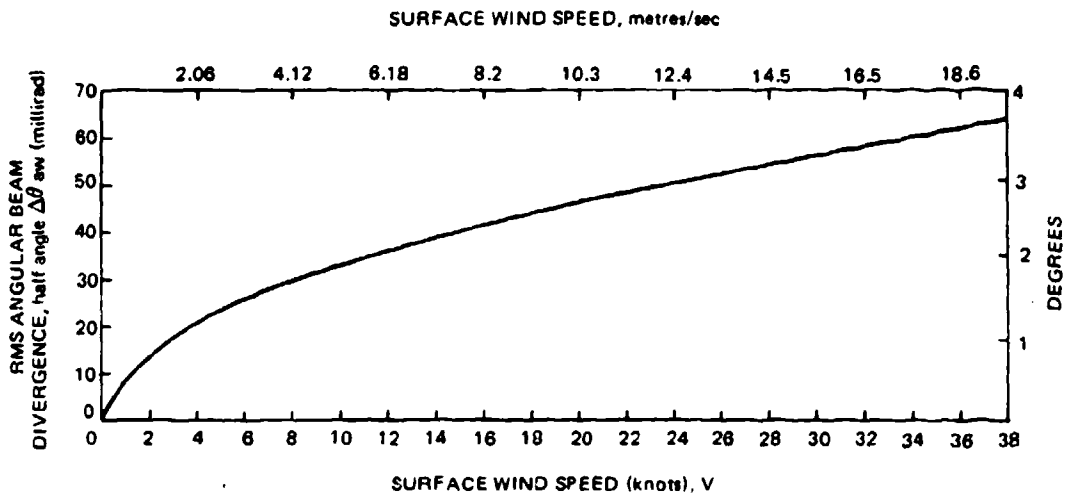

Figure 27. Rms air-water interface effect as a function of wind speed v.

Since the full angular subtense of the sun (and the moon) is ≈0.5 degrees, this effect will substantially increase its apparent size. The relative contribution of $\Delta\theta_{aw}$ to the distribution of noise radiance at the receiver is discussed in section 3.3.8. Except for the clearest water it is a small effect, and so the impact of neglecting zenith angle effects and dissimilar wave slopes in the downward and crosswind direction may be negligible. We therefore adopt this model until better information is available.

3.3.6 Relative Surface Foam Coverage

The energy transmission of the air-water interface is composed of two factors:

$$\tau'_{aw} = (\tau'_{aw1}) \times (\tau_{aw2}),$$

for

τ'_{aw} = total energy transmission of the air-water interface

τ'_{aw1} = air-water interface transmission due to index of refraction discontinuity;

and,

τ'_{aw2} = air-water interface transmission due to foam and streaks on the water surface.

This section treats τ'_{aw2}, while τ'_{aw1} has been treated in section 3.3.4.

The surface foam coverage and its effects are taken to be independent of the noise source and cloud conditions. As discussed in section 2.3.6, for a foam albedo = 1,

$$\tau'_{aw2} = 1 - (1.2\,(10^{-5}))\, v^{3.3},\ v \leqslant 9 \text{ m/sec}\ , \qquad \text{(N-15a)}$$

and

$$\tau'_{aw2} = 1 - (1.2\,(10^{-5}))\, v^{3.3}\,(0.225v - 0.99),\ v \geqslant 9 \text{ m/sec} \qquad \text{(N-15b)}$$

for

v = surface wind speed in metres/sec.

Equation (N-15a, b) is evaluated in table 18 and figure 28 for v in knots (and metres/second).

Although this model neglects zenith angle effects we shall adopt it pending further experimental work.

Table 18. Air-water energy transmission due to surface foam and streaks (assuming a foam streak albedo = 1).

v, Wind Speed		
knots	metres/sec	τ'_{aw2}
0	0	1
2	1.03	1
4	2.06	1
8	4.12	1
14	7.21	0.99
20	10.3	0.96
26	13.4	0.87
32	16.5	0.66
38	19.6	0.25

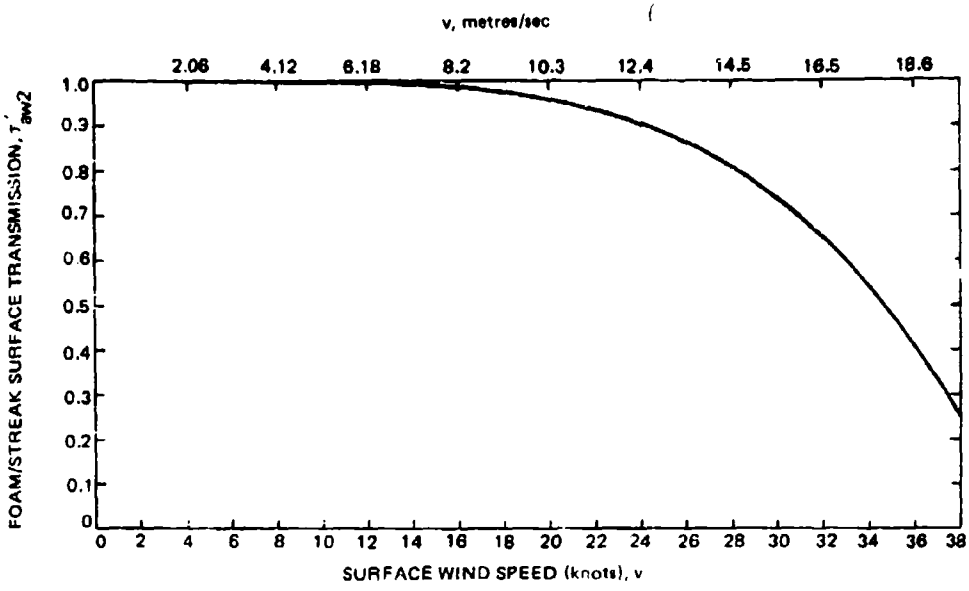

Figure 28. Foam/streak surface coverage transmission versus surface wind speed.

3.3.7 Water Energy Transmission

The energy transmission of the water is denoted by τ'_w. The angularly localized noise sources (sun and moon) behave similarly to the signal energy transmission discussed in section 2.3.7, thus we take:

$$\tau'_{wsu} = \exp - \left\{ \frac{\sum_{i=1}^{j} (k_i D_i)}{\cos \phi_{su}^{w}} \right\} \qquad \text{(N-16)}$$

for

$$\phi_{su}^{w} = \sin^{-1} \left\{ \frac{1}{n} \sin \phi_{su} \right\}$$

and

$$\sum_{i=1}^{j} D_i = D;$$

where,

k_i = diffuse attenuation coefficient for the i'th water layer,

D_i = thickness of the i'th water layer,

D = eceiver depth,

n = sea-water index of refraction,

ϕ^w_{su} = in-water solar zenith angle,

ϕ_{su} = in-air solar zenith angle;

and,

$$\tau'_{wmu} = \exp - \left\{ \frac{\sum_{i=1}^{j} (k_i D_i)}{\cos \phi^w_{mu}} \right\}, \qquad \text{(N-17)}$$

for

$$\phi^w_{mu} = \sin^{-1} \left\{ \frac{1}{n} \sin \phi_{mu} \right\}$$

and

$$\sum_{i=1}^{j} D_i = D \quad .$$

Here,

ϕ^w_{mu} = in-water lunar zenith angle;

ϕ_{mu} = in-air lunar zenith angle.

For the diffuse or uniform, background sources, such as the blue sky and the stars, we assume there is no zenith angle dependence; and so,

$$\tau'_{wb} = \exp - \sum_{i=1}^{j} (k_i D_i) \quad , \qquad \text{(N-18)}$$

and

$$\tau'_{wz} = \exp - \sum_{i=1}^{j} (k_i D_i) \quad . \qquad \text{(N-19)}$$

We do not distinguish here between clear sky, thin cloud, and thick cloud models. This model is uncertain, in

(1) the values of k_i to use,

(2) the values of D_i, and

(3) its applicability in very clear water and/or at shallow receiver depths.

It is the best model available now and it will be revised when better information becomes available.

3.3.8 Water Distribution of Radiance

There is no experimentally verified expression for the in-water distribution of background radiance as a function of source character, source zenith angle, water properties and receiver depth. As discussed in section 2.3.8, we therefore adopt the expression

$$1 - \left(\frac{\sin \phi^{w}}{\sin \phi_0} \right)^2 ,$$

as an estimate of the angular distribution, with

ϕ^{w} = in-water angle measured from the axis, or principal ray of the noise source.

Here, ϕ_0 is related to the half-power point of the received radiance by the equation,

$$\frac{1}{2} = \frac{1 - (\cos \phi_{1/2}) - \frac{1}{3 \sin^2 \phi_0} \left\{ \cos (\phi_{1/2}) \sin^2 (\phi_{1/2}) + 2 \cos (\phi^{1/2}) - 2 \right\}}{1 - \cos \phi_0 - \frac{1}{3 \sin^2 \phi_0} \left\{ \cos \phi_0 \sin^2 \phi_0 + 2 \cos \phi_0 - 2 \right\}} \qquad \text{(N-20a)}$$

Equation (N-20a) is evaluated in table 19. Values between those shown are obtained by linear interpolation.

Table 19. Relation of radiance zero point, ϕ_0, and received radiance half-power point, $\phi_{1/2}$, for $1 - (\sin \phi^{w} / \sin \phi_0)^2$ radiance distribution.

$\phi_{1/2}$ (degrees)	$\phi_{1/2}$ (degrees)
3.8	5
7.6	10
11.4	15
15.2	20
19.0	25
22.7	30
26.5	35
30.2	40
33.9	45
37.5	50
41.1	55
44.6	60
48.1	65
51.6	70
54.9	75
58.2	80

Again, assuming that the in-air incident beam spread, air-water beam spread, and in-water scattering induced spread are *statistically* independent effects, we adopt the NOSC (ref 7) model:

$$\boxed{\phi_{1/2} = [f_w + f_{aw} + f_a]^{1/2} \quad ,} \qquad \text{(N-20b)}$$

for all four out-of-water background sources. For solar and lunar sources,

$$\boxed{f_w = \text{water contribution} \\ = \theta_{si}^2 \frac{s\,D}{\cos \phi_{su}^w} \quad , \text{ all } \tau_{opt}} \qquad \text{(N-21a)}$$

and

$$f_w = \theta_{si}^2 \frac{s\,D}{\cos \phi_{mu}^w} , \text{ all } \tau_{opt} \; ; \qquad \text{(N-22a)}$$

while, for the distributed background sources of blue sky and stellar/zodiacal light,

$$f_w = \theta_{si}^2 \, sD \quad , \quad \text{all } \tau_{opt} \; . \qquad \text{(N-23a)}$$

Here,

θ_{si}^2 = mean square single scattering angle in water,

s = scattering coefficient in water,

D = receiver depth,

ϕ_{su}^w = in-water solar zenith angle, and

ϕ_{mu}^w = in-water lunar zenith angle.

Again, for solar and lunar sources,

$$\boxed{f_{aw} = (0.0103\, v^{1/2})^2 \quad , \quad \tau_{opt} \leqslant 10} \qquad \text{(N-21b), (N-22b)}$$

$$\boxed{= 0 \quad , \quad \tau_{opt} \geqslant 10 \quad .} \qquad \text{(N-21c), (N-22c)}$$

V = surface wind speed (knots), as discussed in section 4.3.5 For the distributed sources,

$$f_{aw} = 0 \quad , \quad \text{all } \tau_{opt} \; . \qquad \text{(N-23b)}$$

Finally, for the sun and moon,

$$f_a = \left(\frac{1}{n}\right)^2 \left(\theta_{s/2}\right)^2 \quad , \quad \tau_{opt} \leq 10 \qquad \text{(N-21d)}$$

$$= (33.8°)^2 \quad , \quad \tau_{opt} \geq 10 \; ; \qquad \text{(N-21e)}$$

and

$$f_a = \left(\frac{1}{n}\right)^2 \left(\theta_{m/s}\right)^2 \quad , \quad \tau_{opt} \leq 10 \qquad \text{(N-22d)}$$

$$= (33.8°)^2 \quad , \quad \tau_{opt} \geq 10 \; . \qquad \text{(N-22e)}$$

Here,

n = water index of refraction,

$\theta_{s/2}$ = half the angular substense of the sun ($\sim(1/4)°$), and

$\theta_{m/2}$ = half the angular substense of the moon ($\sim 1/4)°$).

These equations have been discussed and derived in section 2.3.8. For the distributed sources,

$$f_a = (33.8°)^2 \quad , \quad \text{all } \tau_{opt} \; .$$

In general, the receiver will be directly viewing the signal, while the background source enters at an off-axis angle. Then, the fraction of the noise radiance which enters the receiver is given by

$$f(\phi_o, \theta_R, \delta) = \frac{\int_o^{2\pi} d\theta \int_o^{\theta_R} d\phi^w \sin\phi^w \left[1 - \left(\frac{\sin\phi^{w'}}{\sin\phi_0}\right)^2\right]}{\int_o^{2\pi} d\theta \int_o^{\phi_o} d\phi^w \sin\phi^w \left[1 - \left(\frac{\sin\phi^w}{\sin\phi_0}\right)^2\right]} \; , \qquad \text{(N-24a)}$$

for

$$\phi^{w'} = \cos^{-1} \left| \cos\phi^w \cos\delta + \sin\phi^w \sin\delta \sin\theta \right| \quad ;$$

where,

θ_R = half-angle of the receiver field of view,

δ = off-set angle between axis of noise source and receiver optical axis.

This expression will be used further in section 3.2.10 and 3.2.11.

Equation (N-24a) applies to the background sources in thin cloud conditions. Under thick cloud conditions, both signal and background will appear to arrive from the zenith, and so $\delta \to 0$. For this case,

$$f(\phi_0, \theta_R) = \frac{1 - \cos\theta_R - \frac{1}{3\sin^2\phi_0}\left[\cos\theta_R \sin^2\theta_R + 2\cos\theta_R - 2\right]}{1 - \cos\phi_0 - \frac{1}{3\sin^2\phi_0}\left[\cos\phi_0 \sin^2\phi_0 + 2\cos\phi_0 - 2\right]} \quad \text{(N-24b)}$$

3.3.9 Detection Bandwidth

The required electrical detection bandwidth to optimally detect the pulses discussed in section 2.3.9 is not known at present. In lieu of such a result we assume:

1) The receiver has foreknowledge of the expected pulse width, and

2) $$\boxed{B = \frac{0.4}{(2.45\ t_m)}\ ;} \quad \text{(N-25)}$$

for,

B = electrical detection bandwidth,

t_m = time at which pulse peak value occurs after pulse start, for a pulse shape $f(t) = t \exp - (t/t_m)$.

For gaussian shaped pulses and the detection filter, equation (N-25) is the nearly optimum match.* As further work is done in the area of the real pulses to be expected here, (N-25) may be revised.

Equation (N-25) is evaluated in table 20 and figure 29 for the pulse widths and optical thicknesses developed in section 2.3.9.

---

*H.P. Westman, Editor, Reference Data for Radio Engineer, Fifth Edition, p. 29-5, (H.W. Sams & Co., New York, 1969).

Table 20. Typical detection bandwidths for pulse width conditions of table 11.

τ_{opt}, Optical Thickness	T Geom. Thickness (km)	Δt_c Pulsewidth (μsec)	Δt_m Peak Time (μsec)	B Detection Bandwidth (kHz)
10	0.25	1.15	0.47	348
20	0.5	3.55	1.49	110
30	0.75	7.08	2.89	56.5
40	1.00	11.27	4.6	35.5
50	1.25	16.13	6.58	24.8
60	1.50	21.55	8.8	18.6
70	1.75	27.48	11.22	14.6
80	2.00	33.93	13.85	11.8
90	2.25	40.88	16.69	9.8
100	2.50	48.25	19.7	8.3

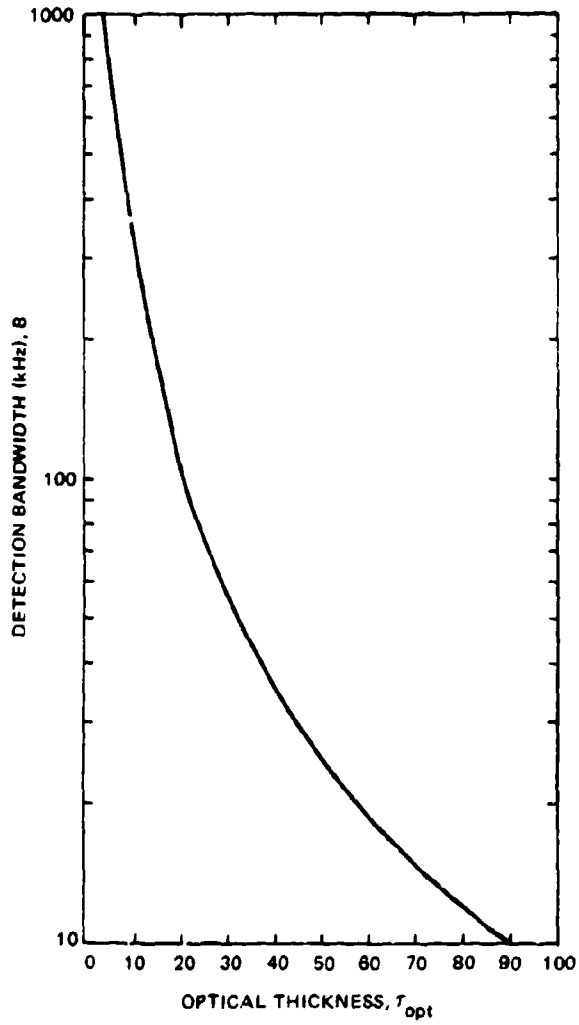

Figure 29. Detection bandwith for pulse-widths of table 11.

3.3.10 Average Background Power Due to Sunlight

The average optical background power in the receiver due to the sun is given by an equation analogous to that developed in section 2.3.10 for the received optical signal energy. We therefore take

P_{su} = (spectral irradiance above the atmosphere due to sun),
× (clear atmospheric transmission) × (cloud transmission)
× (cloud to water transmission)
× (air-water interface transmission) × (water transmission)
× (receiver optics transmission)
× (fraction of incident radiance within receiver field-of-view)
× (area of the receiver). (N-26)

We also take

$H_{s\lambda}$ ≡ exo-atmospheric spectral solar irradiance,
B_{opt} ≡ spectral bandwidth of receiver,
γ_R = receiver optics transmission,
d = diameter of receiver aperture,
$(\pi d^2/4)$ = area of receiver, (N-27)
τ_a = clear atmosphere energy transmission as discussed in section 2.3.1,
τ_c = cloud energy transmission as discussed in section 2.3.2,
τ_{cw} = cloud to water energy transmission as discussed in section 2.3.3,
τ_{aw} = air-water interface energy transmission as discussed in sections 2.3.4 and 2.3.6,
τ_w = water energy transmission as discussed in section 2.3.7, and
$I(\phi^w)$ = water radiance distribution, as discussed in section 2.3.8.

Therefore, the received optical power is given by

$$P_{su} \approx H_{s\lambda} B_{opt} (\pi d^2/4) \gamma_R) \tau_a \tau_c \tau_{cw} \tau_{aw} \tau_w f(\phi_o, \theta_R) \quad \text{(N-28)}$$

The fraction of the incident radiance within the receiver field-of-view is given by (for perfect alignment between beam axis and receiver axis):

$$f(\Omega) = \frac{\int_0^{2\pi} \int_0^{\theta_R} I(\phi^w)\, d\Omega}{\int_0^{2\pi} \int_0^{\phi_o} I(\phi^w)\, d\Omega}, \quad \theta_R \leq \phi_o \quad \text{(N-29)}$$

for

θ_R = half-angle of the receiver field-of-view

ϕ_o = off-axis angle at which incoming radiance equals zero.

Using the model adpted in section 2.3.8,

$$f(\theta_R, \phi_w) = \frac{1 - \cos\theta_R - (\phi_o)^{-2}\left|2\theta_R \sin\theta_R - (\theta_R^2 - 2)\cos\theta_R - 2\right|}{1 - \cos\phi_o - (\phi_o)^{-2}\left|2\phi_o^2 \sin\phi_o - (\phi_o^2 - 2)\cos\phi_o - 2\right|}, \quad \text{for } \theta_R \leq \phi_o \ ; \tag{N-30}$$

and

$$f(\theta_R, \phi_o) = 1 \ , \quad \text{for } \theta_R > \phi_o \ . \tag{N-31}$$

3.3.11 Average Background Power Due to Moonlight

The average optical background power in the receiver due to the moon is completely analogous to that for the sun discussed in section 3.3.10. We therefore take

P_{mu} = (spectral lunar irradiance outside the atmosphere)
X (area of the receiver)
X (clear atmospheric transmission) X (water transmission)
X (cloud to water transmission)
X (air-water interface transmission) X (water transmission)
X (receiver optics transmission)
X (fraction of incident radiance within receiver field-of-view). (N-32)

We take

$H_{mu\lambda}$ ≡ exo-atmospheric lunar irradiance,

B_{opt} ≡ spectral bandwidth of receiver,

γ_R = receiver optics transmission,

d = diameter of receiver aperture,

τ_a = clear atmosphere energy transmission as discussed in section 2.3.1,

τ_c = cloud to energy transmission as discussed in section 2.3.2,

τ_{cw} = cloud to water energy transmission as discussed in section 2.3.3,

τ_{aw} = air-water interface energy transmission as discussed in sections 2.3.4 and 2.3.6,

τ_w = water energy transmission as discussed in section 2.3.7, and

$I(\phi^w)$ = water radiance distribution as discussed in section 2.3.8.

Therefore, the received optical energy is given by

$$P_{mu} = H_{mu\lambda}\, B_{opt} \left(\frac{\pi d^2}{4}\right) \tau_a \tau_c \tau_{cw} \tau_{aw} \tau_w f(\phi_o, \theta_R), \tag{N-33}$$

with

$$\frac{\pi d^2}{4} \tag{N-34}$$

being the area of the detector:

$$f(\Omega) = \frac{\int_o^{2\pi} \int_o^{\theta_R} I(\phi^w)\, d\Omega}{\int_o^{2\pi} \int_o^{\phi_o} I(\phi^w)\, d\Omega} \quad , \quad \theta_R \leq \phi_o \quad . \tag{N-35}$$

Here,

θ_R = half-angle of the receiver field-of-view,

ϕ_o = off-axis angle at which incoming radiance equals zero.

Using the model adopted in section 2.3.8,

$$f(\Omega) = f(\phi_w, \theta_R) = \frac{1 - \cos\theta_R - (\phi_o)^{-2}\left[2\theta_R \sin\theta_R - (\theta_R^2 - 2)\cos\theta_R - 2\right]}{1 - \cos\phi_o - (\phi_o)^{-2}\left[2\phi_o^2 \sin\phi_o - (\phi_o^2 - 2)\cos\phi_o - 2\right]} \tag{N-36}$$

$$\text{for } \theta_R \leq \phi_o \ ;$$

and

$$f(\phi_o, \theta_R) = 1 \quad , \quad \text{for } \theta_R > \phi_o \ ; \tag{N-37}$$

3.3.12 Average Background Power Due to Blue Skylight

The average optical background power in the receiver due to the blue skylight is partially analogous to that for the sun and moon discussed in sections 3.3.10 and 3.3.11. We therefore take, for the average optical background power due to blue skylight:

P_{BS} = (spectral radiance at receiver aperture due to the blue sky)

X (receiver optics transmission) X (receiver area)

X (receiver optical filter bandpass) X (receiver solid angle)

X (fraction of incident radiance within the receiver field of view). (N-38)

We also take

γ_R = receiver optics transmission,

d = receiver aperture diameter,

$\frac{\pi d^2}{4}$ = area of receiver aperture,

B_{opt} = receiver optical filter bandpass,

θ_R = half-angle of the receiver field-of-view,

$2\pi(1 - \cos\theta_R)$ = receiver field-of-view solid angle,

L_{BS} = spectral radiance at receiver aperture due to the blue skylight,

$f'(\phi_O, \theta_R, \delta)$ = fraction of incident radiance within receiver field of view, and

$$P_{BS} = L_{BS} \left(\gamma_R \left(\frac{\pi d^2}{4} \right) \right) B_{opt}\, 2\pi(1 - \cos\theta_R)\, f'(\phi_O, \theta_R, \delta). \qquad \text{(N-39)}$$

Because the blue skylight is a cw source, we use the energy transmission formalism to develop the expression:

L_{BS} = (clear sky exo-atmospheric effective radiance)

X (clear atmospheric transmission) X (cloud energy transmission)
X (cloud to water energy transmission)
X (air-water interface energy transmission) X (water energy transmission); (N-40)

and we use

L_B = clear sky exo-atmospheric effective radiance,

τ'_a = clear atmospheric transmission as discussed in section 3.3.1,

τ'_{CB} = cloud energy transmission as discussed in section 3.3.2,

τ'_{cw} = cloud to water energy transmission as discussed in section 3.3.3,

τ'_{awB} = air-water energy transmission as discussed in sections 3.3.4 and 3.3.6, and

τ'_{wB} = water energy transmission as discussed in section 3.3.7.

Gathering the expressions, we find

$$L_{BS} = L_B\, \tau_a\, \tau_{cb}\, \tau_{cw}\, \tau_{awB}\, \tau_{wB}. \qquad \text{(N-41)}$$

Again, the fraction of blue-sky radiance within the receiver field of view is given by

$$f'(\theta_R, \phi_0, \delta) = \frac{\int_0^{2\pi} d\theta \int_0^{\theta_R} d\phi^w \sin\phi^w \left[1 - \left(\frac{\sin\phi^{w'}}{\sin\phi_0}\right)^2\right]}{\int_0^{2\pi} d\theta \int_0^{\phi_0} d\phi^w \sin\phi^w \left[1 - \left(\frac{\sin\phi^w}{\sin\phi_0}\right)^2\right]} \qquad \text{(N-42)}$$

for

$$\phi^{w'} = \cos^{-1}\left[\cos\phi^w \cos\delta_{BR} + \sin\phi^w \sin\delta_{BR} \sin\theta\right] , \qquad \text{(N-43)}$$

and

δ = off-zenith pointing angle of the receiver axis,

while

ϕ_0 = off-zenith angle at which the blue sky radiance goes to zero.

These expressions will be used in the development of the noise equivalent optical power expression in section 3.3.15.

3.3.13 Average Background Power Due to Stellar/Zodiacal Light

The average optical background power in the receiver due to the nighttime distributed sources of stellar or zodiacal light follows the patterns established in the previous three sections. We take, for the average optical background power due to these sources:

P_Z = (spectral radiance at receiver aperture due to the stellar/zodiacal light)
× (receiver optics transmission) × (receiver area)
× (receiver optical filter bandpass) × (receiver sold angle)
× (fraction of incident radiance within the receiver field-of-view). (N-44)

We again take

γ_R = receiver optics transmission,

d = receiver aperture diameter,

$\frac{\pi d^2}{4}$ = area of receiver aperture,

B_{opt} = receiver optical filter bandpass,

θ_R = half-angle of the receiver field-of-view,

$2\pi(1 - \cos\theta_R)$ = receiver field-of-view solid angle,

L_{ZS} = spectral radiance at receiver aperture due to the steller/zodiacal light,

$f'(\phi_o, \theta_R, \delta)$ = fraction of incident radiance within the receiver field-of-view, and

ϕ_o = off-axis angle at which the received radiance goes to zero, as discussed in section 3.3.8.

Then,

$$P_Z = L_{ZS} \left(\gamma_R \left(\frac{\pi d^2}{4} \right) \right) B_{opt} \ (2\pi(1 - \cos \theta_R)) \ f'(\phi_o, \theta_R, \delta) . \qquad \text{(N-45)}$$

Because this background source is cw, we use the energy transmission formalism to develop the expression:

L_{ZS} = (stellar/zodiacal light clear sky effective exo-atmospheric radiance)

× (clear atmospheric transmission) × (cloud energy transmission)

× (cloud to water energy transmission)

× (air-water interface energy transmission)

× (water energy transmission). (N-46)

We also use,

L_Z = stellar/zodiacal light clear sky effective exo-atmospheric radiance,

τ'_a = clear atmospheric transmission as discussed in section 3.3.1,

τ'_{cz} = cloud energy transmission as discussed in section 3.3.2,

τ'_{cw} = cloud to water energy transmission as discussed in section 3.3.3,

τ'_{awz} = air-water interface energy transmission as discussed in sections 3.3.4 and 3.3.6, and

τ'_{wz} = water energy transmission as discussed in section 3.3.7.

Gathering the expressions we find:

$$L_{ZS} = L_Z \tau'_a \tau'_{cz} \tau'_{cw} \tau'_{awz} \tau'_{wz} . \qquad \text{(N-47)}$$

Again, the fraction of stellar/zodiacal radiance within the receiver field-of-view is given by

$$f'(\theta_R, \phi_o, \delta) = \frac{\int_0^{2\pi} d\theta \int_0^{\phi_0} d\phi^w \sin \phi^w \left[1 - \left(\frac{\sin \phi^{w'}}{\sin \phi_0} \right)^2 \right]}{\int_0^{2\pi} d\phi \int_0^{\phi_0} d\phi^w \sin \phi^w \left[1 - \left(\frac{\sin \phi^w}{\sin \phi_0} \right)^2 \right]}, \qquad \text{(N-48)}$$

for

$$\phi^{w'} = \cos - 1 \left[{}^w\cos \phi^w \cos \delta \quad + \sin \phi^w + \sin \delta \quad \sin \theta \right]$$

and

δ = Off-zenith pointing angle of the receiver axis.

These expressions will be used in the development of the noise equivalent optical power expression in section 3.3.15.

3.3.14 Average Background Power Due to Bioluminescence

The final source of optical background power is the local bioluminescent sources which are stimulated to emit by the submarine motion, or other disturbances in the water. This is modeled in a slightly different way than the previous four sources, and cloud and water properties have only an indirect effect on this source strength. We therefore write for the average background power due to bioluminescence,

P_{BL} = (spectral irradiance at receiver aperture due to bioluminescence)
X (receiver optics transmission) X (receiver area)
X (receiver optical filter bandpass); (N-50)

and we set

L_{BL} = spectral irradiance at receiver aperture due to bioluminescence,

γ_R = receiver optics transmission,

d = diameter of receiver aperture,

$\frac{\pi d^2}{4}$ = area of receiver aperture, and

B_{opt} = optical filter bandpass.

Therefore,

$$P_{BL} = L_{BL} \left(\gamma_R \left(\frac{\pi d^2}{4} \right) \right) B_{opt} \quad \text{(N-51)}$$

3.3.15 Noise Equivalent Optical Power Dependence on Noise Sources

In general, a direct detection optical communication system has four independent noise contributions which include thermal (or amplifier) noise, dark current detector noise, signal shot noise, and background shot noise. These are noise sources insofar as they generate fluctuations in the electrical current present in the detection system. It is conventional to write the "noise" as the 1-σ point of the fluctuating electrical current, assuming the noise sources add independently and are steady in character.

Because we have derived a signal level in terms of the instantaneous received optical power, it is appropriate to describe the noise components in terms of a noise equivalent (optical) power, as derived from the post-detection electrical power.

Ultimately, we write, for a photomultiplier tube type of detector,

$$NEP_{tot} = \left[NEP_{th}^2 + NEP_{dc}^2 + NEP_{ss}^2 + NEP_B^2 \right]^{1/2} ; \quad \text{(N-52)}$$

for,

NEP_{tot} = total noise equivalent (optical) power due to all sources,

NEP_{th} = noise equivalent optical power due to thermal or amplifier noise,

NEP_{dc} = noise equivalent optical power due to photo-detector dark current,

NEP_{ss} = noise equivalent optical power due to shot-noise generated by the signal, and

NEP_B = noise equivalent optical power due to shot-noise generated by the background.

Then,

$$NEP_{TH} = \left[\frac{4\,(kT)\,B\,F_a}{G^2 \left(\frac{\eta e}{h\nu}\right)^2 R_L} \right]^{1/2} ; \qquad \text{(N-53)}$$

for,

(kT) = thermal noise energy = (Boltzman's constant) X (absolute temperature),

B = electrical detection bandwidth as discussed in section 3.3.9,

G = detection gain,

η = photo surface quantum efficiency,

e = charge on the electron,

$h\nu$ = energy per signal photon,

$\eta e/h\nu$ = photo-surface responsivity,

R_L = load resistance, and

F_a = amplifier noise figure.

For the dark current contribution,

$$NEP_{DC} = \left[\frac{2\,e\,B\,F\,G^2\,I_d\,R_L}{G^2\,(\eta e/h\nu)^2\,R_L} \right]^{1/2} = \left[\frac{2\,e\,B\,F\,P_R}{(\eta e/h\nu)^2} \right]^{1/2} ; \qquad \text{(N-54)}$$

for,

F = excess noise in the detector gain

and

I_d = dark current at the photo-cathode.

For the signal shot noise contribution,

$$NEP_{ss} = \left[\frac{2\, e\, B\, F\, (n e/h\nu)\, G^2 P_R\, R_L}{G^2 \eta (e/h\nu)^2\, R_L} \right]^{1/2} = \left[\frac{2\, e\, B\, F\, \hat{P}_R}{(\eta e/h\nu)} \right]^{1/2} ; \qquad \text{(N-55)}$$

for $\hat{P}_R$ = peak received optical signal power at the photo surface, as discussed in section 2.3.10.

Finally, the cw background contributes

$$NEP_B = \left[\frac{2\, e\, B\, F\, G^2\, (\eta e/h\nu)\, R_L \left(\sum_i P_B^i \right)}{G^2\, (\eta e/h\nu)^2\, R_L} \right]^{1/2} = \left[\frac{2\, e\, B\, F \sum_i P_B^i}{(\eta e/h\nu)} \right]^{1/2} ; \qquad \text{(N-56)}$$

for

$$\sum_i P_B^i = P_{su} + P_{mu} + P_{BS} + P_Z + P_{BL} , \qquad \text{(N-57)}$$

where (see fig. 20, page 47/48)

P_{su} = average background power due to sunlight as discussed in section 3.3.10, (N-27);

P_{mu} = average background power due to moonlight as discussed in section 3.3.11, (N-33);

P_{BS} = average background power due to blue skylight as discussed in section 3.3.12, (N-39);

P_Z = average background power due to stellar/zodiacal light as discussed in section 3.3.13, (N-45);

and

P_{BL} = average background power due to bioluminescence as discussed in section 3.3.14, (N-51).

Two comments are in order at this point.

1. If the signal shot noise dominates the noise components, the formulation should be re-examined to insure that enough photo-electrons are being generated to make it applicable.
2. Not all the average background contributors will be present at any one time, which will be accounted for in the time-of-day modeling of the respective spectral radiances.

REFERENCES

1. AFCRL-71-0279, Optical Properties of the Atmosphere (revised), RA McClatchey, RW Fenn, JEA Selby, FE Volz, and JS Garing, Unclassified, 10 May 1971.

2. EA Bucher, Computer Simulation of Light Pulse Propagation for Communication Through Thick Clouds, Appl Optics, Vol 12 (10), p 2391–2400, October 1973.

3. RE Danielson, DR Moore, and HC Van de Hulst, The Transfer of Visible Radiation Through Clouds, J Atmos Sci, Vol 26 (9), p 1078–1087, September 1969.

4. NOSC TN 279, A Test Plan for Determining the Feasibility of Optical Satellite Communications Through Clouds at Visible Frequencies (U), S Karp, Unclassified, appendix B equation (14), 1 July 1978.

5. J Gordon, Directional Radiance (Luminescence) of the Sea Surface, SIO, ref 89-20, October 1969.

6. C Cox and W Munck, Statistics of the Sea Surface Derived from Sun Glitter, J Marine Res, Vol 13 2, 1954.

7. NELC TR 2021, Submarine-Aircraft and Submarine-Satellite Optical Communications Systems Model (U), RE Howarth, ME Hyde, and WR Stone, Confidential, 1977.

8. HR Gordon and MM Jacobs, Albedo of the Ocean-Atmospheric System: Influence of the Sea Foam, Appl Optics, Vol 16 (8), p 2257–2260, August 1977.

9. LB Stotts, Closed Form Expression for Optical Pulse Broadening in Multiple Scattering Media, Appl Optics, Vol 17 (4), p 504–505, 15 February 1978.

10. Handbook of Geophysics (rev ed), p 17-1, 17-2, MacMillan Co, New York, 1960.

11. RC Haynes, Introduction to Space Service, p 4–5, John Wiley and Sons, New York, 1971.

12. WK Pratt, Laser Communication Systems, ref 4, p 122, fig 6–7, John Wiley and Sons, New York, 1969.

13. NOSC Interim Report No. 2, Contract No. N00039-77-C-0100, Optical Submarine Communication by Aerospace Relay (OSCAR) (U), T Flom, PJ Titterton, et al, p 3-22 to 3-24, Secret, 1 May 1978.

14. Handbook of Mathematical Functions, M Abramowitz and IA Stegun, eds, p 228, NBS Applied Mathematics Series 35, GPO, November 1970.

GLOSSARY

This glossary defines all the English and Greek symbols used in the Naval blue-green downlink model. The English symbols are listed alphabetically, followed by the Greek symbols.

ENGLISH SYMBOLS

A A_E = Energy to instantaneous power normalization parameter

B b = Effective clear atmosphere optical thickness

B = Electrical detection bandwidth

B_{opt} = Receiver optical filter bandpass

C C_f = Fraction of sea-surface covered by foam and streaks

c = Speed of light

D D = Receiver depth

D_i Thickness of i'th water layer

d = Diameter of receiver aperture

E E_R = Total received energy per pulse

exp = Exponential

E_p = Transmitted energy per pulse

e = Charge on the electron

E_2 = Exponential integral

F f_w = Water contribution to received beam half-angle

f_{cw} = Air-water interface contribution to received beam half-angle

f_a = Atmospheric contribution to received beam radiance

f_{wi} = Contribution of i'th water layer to received beam half angle

f(t) = Received pulse shape

$f'(\phi_0, \theta_R)$ = Fraction of incident radiance within receiver field of view

$f'(\phi_o, \theta_R, \delta_{su})$ = Fraction of incident radiance within receiver field of view

F = Excess noise in detector gain

F_a = Amplifier noise figure

G G = Detection gain

H H = Distance from cloud base to water surface

$h\nu$ = Energy per signal photon

I $I(\phi^W)$ = Water radiance distribution

I_d = Dark current at the photo-cathode

J j = Number of water layers present from surface to submarine receiver

K k = Diffuse attenuation coefficient of the water

k_i = Diffuse attenuation coefficient of i'th water layer

(kt) = Thermal noise energy = (Boltzmann's constant) X (absolute temperature)

L L_{SU} = Spectral radiance at receiver aperture due to the sun

L_S = Exo-atmospheric effective solar radiance

L_{MU} = Spectral radiance at receiver aperture due to the moon

L_m = Exo-atmospheric effective lunar radiance

L_{BS} = Spectral radiance at receiver aperture due to blue skylight

L_B = Clear sky exo-atmospheric effective radiance due to blue skylight

L_{ZS} = Spectral radiance at receiver aperture due to stellar and zodiacal light

L_Z = Clear sky exo-atmospheric effective radiance due to stellar and zodiacal light

L_{DL} = Spectral irradiance at receiver aperture due to bioluminescence

N n = Water index of refraction

NEP_{tot} = Total noise equivalent optical power due to all sources

NEP_{TH} = Noise equivalent optical power due to thermal or amplifier noise

NEP_{DC} = Noise equivalent optical power due to photo-detector dark current

NEP_{SS} = Noise equivalent optical power due to shot-noise generated by the signal

NEP_B = Noise equivalent optical power due to shot-noise generated by the background

P $P_R(t)$ = Instantaneous received signal power

P_{su} = Average optical power at receiver due to the sun

P_{mu} = Average optical power at receiver due to the moon

P_{BS} = Average optical power at receiver due to the blue sky

P_Z = Average optical power at receiver due to stellar and zodiacal light

P_{BL} = Average optical power at receiver due to bioluminescence

$\hat{P}_R$ = Peak received signal power

Q q = Parameter describing ability of satellite transmitter to correct for zenith angle spot spreading. $0 \leq q \leq 1$

R — R = Range from satellite to submarine

R_L = Load resistance

S — s = Water scattering coefficient

s_i = Scattering coefficient of i'th water layer

T — T = Geometrical thickness of the cloud

t = Time

t_m = Time after pulse start at which peak value occurs

Δt_w = Pulse width due to water portion of the path

Δt_{cw} = Pulse width due to cloud to water portion of the path

Δt_c = Pulse width due to cloud portion of the path

U

V — v = Surface wind speed

W

X

Y

Z

GREEK SYMBOLS

The Greek symbols are listed in order according to the Greek alphabet: $\alpha, \beta, \gamma, \delta, \epsilon, \zeta, \eta, \theta, \iota, \kappa, \lambda, \mu, \nu, \xi, o, \pi, \rho, \sigma, \tau, \upsilon, \phi, \chi, \psi, \omega$.

α

β

γ — γ_T = Transmitter optics transmission

γ_R = Receiver optics transmission

δ — δ = Off-set angle between receiver optical axis and axis of the incoming light

ϵ

ζ

η

θ θ = Cloud particle mean scattering angle

$\langle \cos\theta \rangle$ = Mean cosine of the in-cloud scattering angle

θ_T = Full angle exp (-2) transmitter beamwidth

$\Delta\theta_{AW}$ = Rms half-angle additional signal beam divergence due to wave action

θ_{Si}^2 = Mean square single scattering angle in water

θ_{Sij}^2 = Mean square single scattering angle in water for the j'th water layer

θ_R = Half angle of the receiver field of view

$\Delta\theta_{AW}^{SU}$ = Rms half-angle air-water interface induced spread for the sunlight

$\Delta\theta_{AW}^{MU}$ = Rms half-angle air-water interface induced spread for the moonlight

$\theta_{S/L}$ = Half the angle subtended by the sun

$\theta_{M/L}$ = Half the angle subtended by the moon

$\Delta\theta_{AW}^{B}$ = Rms half-angle air-water interface induced spread for the blue sky light

$\Delta\theta_{AW}^{Z}$ = Rms half-angle air-water interface induced spread for the stellar/zodiacal light

ι

κ

λ

μ

ν

ξ

o

π

ρ

σ σ_c = Mean extinction coefficient of the cloud

τ τ_a = Signal clear atmospheric energy transmission

τ_c = Signal cloud energy transmission

τ_{opt} = Optical thickness of the cloud

τ_{cw} = Signal cloud to water energy transmission

τ_{aw} = Signal total energy transmission of air-water interface

τ_{aw1} = Signal air-water interface energy transmission due to the index of refraction discontinuity

τ_{aw2} = Signal air-water interface energy transmission due to foam and streaks on the sea surface

τ_w = Signal water energy transmission

τ'_a = Background clear atmospheric energy transmission

τ'_{cb} = Cloud energy transmission of the blue skylight

τ'_{cs} = Cloud energy transmission of direct sunlight

τ'_{cm} = Cloud energy transmission of the direct moonlight

τ'_{cz} = Cloud energy transmission of the stellar and zodiacal light

τ'_{cw} = Background cloud to water energy transmission

τ'_{aw} = Total background energy transmission of the air-water interface

τ'_{aw1} = Background air-water interface transmission due to index of refraction discontinuity

τ'_{aw2} = Background air-water interface transmission due to foam and streaks on the sea surface

τ'_{awis} = Solar air-water interface transmission due to index of refraction discontinuity

τ'_{awim} = Lunar air-water interface transmission due to index of refraction discontinuity

τ'_{awib} = Blue-skylight air-water interface transmission due to index of refraction discontinuity

τ'_{awiz} = Stellar and zodiacal light air-water interface transmission due to index of refraction discontinuity

τ'_{wsu} = Solar water energy transmission

τ'_{wmu} = Lunar water energy transmission

τ'_{wb} = Blue sky water energy transmission

υ τ'_{wz} = Stellar and zodiacal light water energy transmission

ϕ ϕ_s = Signal in-air zenith angle

ϕ_s^w = Signal in-water zenith angle

ϕ_0 = Off-axis angle at which in-water radiance goes to zero

$\phi_{1/2}$ = Half-power angle of the received signal beam radiance

ϕ_{su} = Solar in-air zenith angle

ϕ_{mu} = Lunar in-air zenith angle

$N^{\phi 1/2}$ = Half-power angle of the background radiance

χ

ψ

ω

ω_0 = sing'e scatter albedo